Earthquake Wave-Soil-Structure Interaction Analysis of Tall Buildings

by

Ming Ming Yao
B.E., Beijing University of Aeronautics and Astronautics, 1999
M.A.Sc., University of Victoria, 2003

A Dissertation Submitted in Partial Fulfillment of the
Requirements for the Degree of

DOCTOR OF PHILOSOPHY

in the Department of Mechanical Engineering

Earthquake Wave-Soil-Structure Interaction Analysis of Tall Buildings

by

Ming Ming Yao
B.E., Beijing University of Aeronautics and Astronautics, 1999
M.A.Sc., University of Victoria, 2003

Supervisory Committee

Dr. Joanne L. Wegner, Supervisor
(Department of Mechanical Engineering)

Dr. James B. Haddow, Departmental Member
(Department of Mechanical Engineering)

Dr. Bradley J. Buckham, Departmental Member
(Department of Mechanical Engineering)

Dr. George D. Spence, Outside Member
(School of Earth and Ocean Sciences)

Supervisory Committee

Dr. Joanne L. Wegner, Supervisor
(Department of Mechanical Engineering)

Dr. James B. Haddow, Departmental Member
(Department of Mechanical Engineering)

Dr. Bradley J. Buckham, Departmental Member
(Department of Mechanical Engineering)

Dr. George D. Spence, Outside Member
(School of Earth and Ocean Sciences)

ABSTRACT

Earthquakes cause damages to structures and result in great human casualties and economic loss. A fraction of the kinetic energy released from earthquakes is transferred into buildings through soils. The investigation on the mechanism of the energy transferring from soils to buildings during earthquakes is critical for the design of earthquake resistant structures and for upgrading existing structures. In order to understand this phenomena well, a wave-soil-structure interaction analysis is presented. The earthquake wave-soil-structure interaction analysis of tall buildings is the main focus of this research. There are two methods available for modeling the soil-structure interaction (SSI): the direct method and substructure method. The direct method is used for modeling the soil and a tall building together. However, the substructure method is adopted to treat the unbounded soil and the tall building separately. The unbounded soil is modeled by using the Scaled Boundary Finite-Element Method (SBFEM), an infinitesimal finite-element cell method, which naturally satisfies the radiation condition for the wave propagation problem. The tall building is modeled

using the standard Finite Element Method (FEM). The SBFEM results in fewer degrees of freedom of the soil than the direct method by only modeling the interface between the soil and building. The SBFEM is implemented into a 3-Dimensional Dynamic Soil-Structure Interaction Analysis program (DSSIA-3D) in this study and is used for investigating the response of tall buildings in both the time domain and frequency domain. Three different parametric studies are carried out for buildings subjected to external harmonic loadings and earthquake loadings. The peak displacement along the height of the building is obtained in the time domain analysis. The coupling between the building's height, hysteretic damping ratio, soil dynamics and soil-structure interaction effect is investigated. Further, the coupling between the structure configuration and the asymmetrical loadings are studied. The findings suggest that the symmetrical building has a higher earthquake resistance capacity than the asymmetrical buildings. The results are compared with building codes, field measurements and other numerical methods. These numerical techniques can be applied to study other structures, such as TV towers, nuclear power plants and dams.

Contents

List of Tables

List of Figures

ACKNOWLEDGEMENTS

I would like to thank:

Dr. Joanne L. Wegner for supporting and guiding me through my graduate study;

Dr. James B. Haddow for the discussions and guidance;

Drs. Bradley J. Buckham and George D. Spence for their suggestions and time;

Dr. Sukhwinder K. Bhullar for the help and encouragement;

Dr. Louise R. Page for offering the opportunity of studying the soil microstructure using the facilities in the Department of Biology;

Mr. Brent Gowen for teaching me using the equipment in the Electron Microscopy Laboratory;

Ms. Heather Down for helping me processing the soil data in the Advanced Imaging Laboratory.

DEDICATION

To Lily and my lovely daughters Wen & Ya.

Chapter 1

Introduction

The earthquake wave-soil-structure interaction analysis of of tall buildings with a symmetrical or an asymmetrical configuration is studied here. The urgency of carrying out such study is stressed again from the devastating aftermath of recent major earthquakes. The collapse of tall apartment buildings, such as in the Izmit, Turkey 1999 earthquake and the Pakistan/India 2005 earthquake, astonished the earthquake engineering and civil engineering communities. The Soil-Structure Interaction (SSI) effect is still not well understood due to the inadequate modeling of soil properties and the radiation condition in an unbounded media. Since the end of last century, the Scaled Boundary Finite-Element Method (SBFEM) has been developed from the idea of similarity, which means taking the limit of the thickness of an infinitesimal finite-element cell along a soil-structure interface. The unbounded half-space soil is modeled in this SBFEM with the radiation condition satisfied naturally. The substructure concept is used for attacking these complex modeling issues involving different type of soils and geometrical characters. The substructure method results in fewer degrees of freedom of the soil in this numerical model compared with a direct method where modeling a large amount of soil adjacent to the building is necessary for satisfying the radiation condition. In this research, the SSI effect on the vibration of tall buildings is investigated in both time and frequency domains. The fundamental frequency, equivalent damping ratio, dynamic response of tall buildings with symmetrical and asymmetrical configuration are provided. The various factors, including the soil types, building heights, the floor plan configuration and loading types are examined for achieving a better understanding of the behaviour of tall buildings during an earthquake.

1.1 Summary of the work

First, references on modeling of tall buildings, unbounded soil, and soil-structure interaction are reviewed. The method for modeling the structure is an important field due to the complexity of modeling the structural elements, such as, the steel-reinforced concrete, the configuration of the core, and the openings in the walls. For research in the field of building vibration, the reader is referred to [21].

In the time domain, the SSI effect on the vibration of tall buildings is analyzed by studying the detailed dynamic responses of symmetrical tall buildings under simulated seismic loadings. The dynamic response of this soil-structure system depends upon frequency content of the ground vibration, type and input angle of ground motion, stiffness and height of the building, the number of levels in its multi-level basement, and the stiffness of the adjacent soil.

In the frequency domain, the SSI effect of buildings with 5-, 10-, 15-, 20-, and 25-stories is modeled. In each case, the fundamental frequency and corresponding radiation damping ratio are obtained. The relationship between the SSI effect and the building height is examined. This relationship is the dominant factor in determining the free vibration of a tall building. A 15-story building is chosen to investigate further the relationship between the material properties of soils and the dynamic response of the building.

Further, the structural response to dynamic loading, which is expressed in terms of displacements of the structure, is studied. A two-way asymmetrical multistory building model is subjected to bidirectional loadings. The time histories of the vertical and horizontal displacements and rotation of the roof are obtained using the SBFEM. The SBFEM, implemented in the 3-Dimensional Dynamic Soil-Structure Interaction Analysis program (DSSIA-3D), takes into account the soil-structure interaction effects and is applied to study two-way asymmetrical buildings. These results are compared with those of symmetrical buildings. Recommendations for improving the seismic design of tall buildings are given from this comparison.

In summary, the work has resulted in the following conclusions:
(1) The vibration of tall buildings with symmetrical or asymmetrical configuration is simulated for harmonic and earthquake loadings. This research confirms the field observation that the largest deformation of buildings occurred at the basement level. P waves cause more deformation and movement along the input direction. Shear waves cause much more inter-story drift and damages.

(2) The influence of different soil types to the earthquake response of tall buildings is investigated. The soil of larger stiffness results in a higher fundamental frequency of the building in a non-linear relationship fashion.
(3) The response of asymmetrical tall buildings is stronger in general than the corresponding symmetrical buildings. This indicates the symmetrical building is more seismic resistant than an asymmetrical building in an earthquake.
(4) The building is modeled with more complex structural features during the course of investigations.

1.2 Introduction

Vibrations of tall buildings are mainly caused by either strong winds or ground motions. In both situations, the mechanism that influences the vibration characteristics of tall buildings is the dynamic Soil-Structure Interaction (SSI), which is mainly governed by soil properties. The boundary condition between the soil and the foundation of the tall building is assumed free. That permits six Degrees-Of-Freedom (DOF): three translational and three rotational DOF for a rigid foundation. The contact between the foundation and the soil is dynamic.

In this study, two types of ground motion are used, harmonic loading and seismic loading. Seismic waves consist of body waves (such as dilatational and shear waves) and surface waves (such as Rayleigh and Love waves). The body waves can strike buildings at any angle in the half-space [2]. The seismic wave is the primary manifestation of the energy released from an earthquake. The energy from the incoming wave is transferred to the building through the interaction with the adjacent soil excited by the wave propagation. The amount of energy transferred to the building is different for waves with different input angles.

In the time domain analysis of this study, the response of the building is represented by the peak displacement of the building geometric centerline, and is given in Chapter 5. The characteristics of the building vibration include, for example, the peak displacement of the building centerline, the maximum stress on the basement wall, and the stress underneath the foundation mat. The contact mechanism between the foundation and supporting soil can be modified for improving the earthquake-resistant design of buildings. This information can be used to assess the vulnerability of an existing building for the purpose of upgrading protection measures.

In an earthquake, the wave reflection from the foundation to the surrounding semi-infinite soil results in energy dissipation. In the SSI system, not all of the outgoing wave energy will be reflected back into the system. This dynamic SSI system is a damping system. The effect of the energy dissipation can be understood by studying the changes of the fundamental frequency and corresponding radiation damping ratio, which means the wave propagating outward will not be reflected back into the soil-structure system. In Chapter 6, a group of tall buildings, ranging from 10- to 25-story, are modeled and their fundamental frequencies and associated radiation damping ratios are calculated. In a parametric study, the material properties of the soil are shown to have influence on the response of the building. In particular, the effects of the structural hysteretic damping ratio and soil stiffness are investigated.

Asymmetrical buildings are more vulnerable to earthquakes than symmetrical buildings. In this study, a two-way asymmetrical 15-story building with one level basement is modeled. The two-way asymmetrical is the result from the mass eccentricity of the building. The location of the mass center is located away from the geometrical center in the first quadrant. Seismic acceleration recordings are applied at the origin of the coordinate system, which is the control point. It is observed that the response of the asymmetrical building is characterized by the magnitude of the dominant peak displacement. The two-way asymmetrical building coupled with the asymmetrical earthquake loadings are studied in chapter 7. These results are compared with the case of symmetrical buildings and verified by references [23] and [59]. This part of research is published in a recent journal paper [90].

Chapter 2

Problem

The earthquake response of tall buildings with symmetrical or asymmetrical configuration is studied here. The dynamic Wave-Soil-Structure Interaction (WSSI) analysis involves studying the earthquake responses of a wide range of structures, such as dams, tall buildings, TV towers, nuclear power plants, buried pipelines and subway tunnels. During major earthquakes, some of the infrastructures can be severely damaged causing devastating consequences to the local economy and society. In strong earthquakes , there could be tens of thousands of fatalities and millions of buildings damaged. For example, in Pakistan/India 2005 earthquake, some residential buildings, including adobe-wall houses, stone masonry, brick masonry, and tall apartment buildings with steel reinforced concrete (SRC) structures, suffered severe damages. In some cases, walls cracked and failed to support the overlying heavy slabs, which caused many fatalities. The collapse of the wall and SRC columns resulted in a toppled or pancaked structures.

However, in the past, especially in some jurisdictions, the structural design codes do not include dynamic design criteria, but simply use the weighted load method. This method cannot guarantee a safe design for resisting earthquakes without undergoing a series of shaking table tests of the building model. In the investigation carried out by Benedetti et al [7], the scaled 1:2 masonry building models were all severely damaged in the shaking table tests. Furthermore, the interaction between soil and structure is far more complicated than what a shaking table can simulate. Also, in the shaking table test, especially for a tall structure, the table-structure interaction must be taken into consideration in interpreting the testing results and can not be considered as a form of foundation-structure interaction or soil-structure interaction [70].

With the increasing computational power and emerging numerical methods, such as the Finite-Element Method (FEM), Boundary-Element Method (BEM), Meshfree Method (MFM) ([6], [40], and [92]) and Scaled Boundary Finite-Element Method (SBFEM) [63], the soil-structure interaction can be effectively modeled and simulated.

In the field of soil-structure interaction research, structures are usually assumed to be elastic and modeled by a standard FEM. However, the soil is an unbounded half-space medium with a nonlinear stress-strain relationship. The soil is also inhomogeneous. The soil is usually composed of rock particles, organic matter and water. The structure of soil is typically made of a solid framework of grains with the interstitial space filled with water and gas. In general, the mechanical properties of soils are influenced by the water content and the type of the solid ingredients in its compositions. The mechanical properties of soil vary in geographic locations, in climate conditions, and in the presence of earthquake waves. There is not a universal constitutive law for soils in every situation [49]. In this present study, the dynamic character of soils will be the dominant factor for choosing a proper soil model. Considering this, the plasticity of soils will not be included in the dynamic studies, even though the plasticity is a very important character of soils for static and quasi-static problems. Thus the modeling of soils becomes a critical issue in the soil-structure interaction analysis.

In this study, the 3-Dimensional Dynamic Soil-Structure Interaction Analysis (DSSIA-3D) program is used [94]. In DSSIA-3D, the SBFEM is used to model the unbounded elastic medium for its theoretical advantages, since the SBFEM satisfies the radiation condition naturally [63]. Further, the soil-structure interaction of a two-way asymmetrical building subjected to 1940 El Centro earthquake loadings is studied. The comparison between this two-way asymmetrical building and the corresponding symmetrical building under the same loadings clearly demonstrates the critical influence of the asymmetrical factor on the earthquake response.

In summary, the objective of this research is to investigate the earthquake response of tall buildings with the soil-structure interaction effect. Both symmetrical and asymmetrical tall buildings are studied and compared with references and field observations ([23] and [59]). The findings are valuable for designing base isolator, mass damper, and structural seismic resistance upgrading. The research also can be extended to study the earthquake response of other structures such as, TV towers, dams, buried pipelines, and underground structures.

Chapter 3

Background

There are many methods for modeling the SSI in the frequency domain (Fourier or Laplace transformation) and the time domain. There are also hybrid methods obtained by combining the Finite Element Method (FEM) [5] and Boundary Element Method (BEM) ([22] and [91]). These include the interfacial FEM, the joint element method, or a simple physical model which adopts the spring-dashpot system for representing the interaction between the soil and structure. The building foundation can be modeled as a massless flexible, or rigid plate either lying on the soil surface or embedded in the soil. The interface between the soil and structure is modeled as joint connection by enforcing the same displacement and stress on the interfacial nodes.

3.1 Modeling of tall buildings

In the 1950's and early 1960's ([19], [25], and [31]), a building was modeled as a cantilever beam. In these early studies, a digital computer was first used to solve the analytical equations for vibration of tall buildings and obtain their natural periods and damping ratios. At that time, the discretization method and massive calculations were not popular yet. The computer speed and memory storage limited the accuracy of approximation and the level of complexity of modeling. The method for modeling structural vibration needed to avoid generating a large number of DOFs and a large size matrix, such as the mass and stiffness coefficient matrix, in the equation of motion. Other methods have been developed in the past few decades. A simple model of the building using coupled shear plates with openings was applied to investigate the shear wall vibrations and mode shapes for a building damaged in the Alaskan

earthquake of 1964 [28]. Under this guideline, other methods such as the finite strip model and the continuum model were developed ([4], [11], and [32]). All of the above methods result in fewer DOFs. The size of the resulting coefficient matrices was small compared with those using FEM for volume discretization. But these methods lose nonlinear information such as the material nonlinearity and geometrical nonlinearity, and usually are applied only to linear elastic structures. Since a slender structure is significantly nonlinear at large deformation, the small deformation assumption is no longer accurate enough. Usually after a strong earthquake, inside structural component failure occurs, such as the failure of welded points and joints between the steel beams, and dislocation between the steel and attached concrete is often found. These material discontinuities can be modeled as uncertainties in some methods [37].

In recent years, the vibration of the tall buildings is of an increasing interest among the research community. The research on the three dimensional structural dynamics of the vibration of the tall buildings in typhoon active areas such as Hong Kong and Singapore proved that monitoring and controlling the vibration of the tall building is essential for providing a comfortable residential environment ([8] and [38]). It is important to compare the natural frequency of one building and the frequency spectrum of the typhoon recorded in situ. Researchers in Japan ([47], [48], and [54]) studied the reduction of the vibration amplitude of a tall building subject to a strong wind load or strong earth motion using a hybrid mass damper system.

Most methods do not include the soil-structure interaction effects when studying the vibration of the building. Some researchers did consider the SSI effects but were limited to a two dimensional analysis [68]. The consideration of the soil-structure interaction effect on the response of the building in three dimensions is necessary to pursue more accurate results from the viewpoint of engineering practice [69].

Asymmetrical buildings are more vulnerable to earthquake hazards compared to the buildings with symmetrical configuration. The recognition of this sensitivity has led researchers to concentrate their studies on earthquake characteristics, evaluation of the structural parameters and validity of the system models ([29], [30], [24], [12], [58], [46], [60]). So far, several researchers have attempted to evaluate the seismic response behaviour of torsionally coupled buildings for the linear analysis of three dimensional dynamic soil-structure interactions of asymmetrical buildings [3]. The influence of dynamic soil-structure interaction on seismic response was studied in [59], selecting a set of reinforced concrete structures with gravitational loads and representative systems designed for earthquake resistance in accordance with current

criteria and methods.

In this study, the soil-structure interaction of a tall building is numerically simulated, and the results are compared with building codes, field measurements and results from other numerical methods. The soil-structure interaction effect is investigated and evaluated in both the time domain and frequency domain. Further, the loading mode and asymmetrical structural configurations are taken into consideration, together with the soil-structure interaction effect.

3.2 Modeling of unbounded soil

Soil constituents exist in solid, liquid and gas states. The solid phase is a mixture of mineral and some organic matter. Soil shows strong nonlinearity in material properties. It is necessary to include the nonlinearity of the soil material in the numerical modeling, such as using a FEM. For a large scale case, improving the accuracy requires a large number of finite elements with smaller dimension. The coefficient matrix of each element is assembled into the total coefficient matrix of the structure. The radiation condition can not be satisfied by the FEM equations without an artificial transmitting boundary. In order to satisfy the radiation condition for wave propagation in the unbounded soil domain, the artificial transmitting boundary behaves as an energy sink for the outgoing waves. In some researches, a linear elastic homogeneous soil is assumed in the problem for large scale structures, such as highrise buildings, dams, and underground lifelines. Using this assumption, the BEM is widely used in modeling unbounded soil with a transmitting boundary for accommodating energy radiation [35]. In earlier studies, ([55] and [15]), it is assumed that the three dimensional wavefield is composed of a free field and a scattered wavefield. The wavefield is given by solving the Navier's equation in terms of spherical Hankel and Bessel functions, associated with Legendre polynomials ([67] and [1]). The radiation condition is satisfied at infinity in the unbounded half-space. But the stress free boundary condition along the surface of the half-space needs to be set locally. In the above methods, the body force is assumed to be equal to zero. Furthermore, the hysteretic damping ratio, which indicates the internal energy loss due to building vibrations, can be included by using the complex elastic constants ([52] and [26]). The steady-state elastodynamic field equation is used to model the soil which is assumed to be a linear elastic solid [10].

The wave expansion method is used for solving the wave equation for unbounded

soil [15]. In this case, a wavefield is expressed as a linear combination of wave functions of a free field and a reflected wavefield. By imposing boundary conditions and free-field stresses on the boundary, the coefficient of displacement can be obtained after solving the equations. Furthermore, the displacement and stress fields can be evaluated. There are no stress tractions on the free boundary which is set locally as in the other methods.

Based on linear elastodynamic theory, a new method was developed by Song and Wolf [62] and is known as the consistent infinitesimal finite-element cell method. The same equation is obtained for the dynamic-stiffness matrix by limiting the cell width derived in the Scaled Boundary Finite-Element Method (SBFEM). In the SBFEM, the dynamic behaviour of a unbounded soil is described by using a dynamic stiffness matrix in the frequency domain and the same force-displacement relationship is represented in the time domain by a unit-impulse response matrix.

3.3 Modeling of soil-structure interaction

Extensive literature has appeared in the last two decades on modeling soil-structure interactions. This problem is modeled from many points of view by using advanced numerical techniques such as FEM, BEM, and hybrid methods. As a whole, all of the above methods involve approximate simulations of the real soil-structure interaction with some simplifications. Each method has its own merit in modeling soil and soil-structure interface. These methods can be divided into the following groups as follows.

3.3.1 The analytical method

Mario E. Rodriguez et. al. [51] evaluated the importance of SSI effects on the seismic response and the damage of buildings in Mexico City during a 1985 earthquake and compared the results with a rigid case. A simple one degree of freedom model was used for analyzing the overall seismic behaviour of multi-story building structures built on soft soil. Wolf also used this method to study the vibration of the foundation [82]. The mass-spring-dashpot system is widely used to model the interaction of the soil and structure. The analytical method can only be applied to simple structures.

3.3.2 The system identification method

Jonathan P. Stewart and Gregory L. Fenves [65] evaluated the unknown properties of a system by using a pair of known inputs and known outputs for the system. In their method, a simple spring-mass system is used for the initial interaction. The equations are solved in the Laplace domain by using the parametric system identification method. This method was developed from Luco's method for non-parametric procedure [42]. Fifty-eight sites with instrumentation were investigated for both flexible and fixed boundary condition cases by the authors. The responses of the systems to the designed inputs were compared and the SSI effects were addressed. The application of the system identification method in the SSI effect research is efficient.

3.3.3 Nonlinear soil-structure interaction analysis

The nonlinearities of the interaction between the soil and structure are contributed by material nonlinearities of the soil and the structure, and geometrical nonlinearity from motions such as separation, sliding, and rocking. These nonlinear phenomena usually occur concurrently. The coupling from the separation, sliding, and rocking are difficult to simulate. In analyzing a nonlinear dynamic response of SSI, the nonlinear impedance method is a modification of the linear impedance method [79]. The time-dependent contact area between the structure base-slab and the soil can be determined ([66] and [50]). The time domain framework is limited to the mat foundation. In [79] and [87], nuclear containment structures including the effects of liftoff and sliding of the basemat foundation were studied. The rocking and normal separation of the foundation and soil is the primary nonlinear interaction effect [50].

In [85], complete equations were given and the uplift was calculated. A unit impulse matrix was obtained for describing the dynamic response of the soil. In [86], the Green function was calculated and Bessel functions were used. The uplift was examined in the time domain by John P. Wolf and Georges R. Darbre [84]. In this study, the boundary element method is used to model an embedded foundation.

Toki and Fu [69] studied a three dimensional stress redistribution of soil based on the Mohr-Coulomb failure law. A generalized method for a full nonlinear earthquake analysis with joint elements was derived for both soil nonlinearity and geometrical nonlinearity, including uplift and sliding.

The dynamic process can be simulated at a series of states calculated in each infinitesimal time interval. Kawakami [36] used an iterative method to simulate the

rocking procedure with the modification of the traction and displacement of the foundation and soil. The contact and partial uplift phenomenon were modeled by using a FE model of the surface rigid foundation under the assumption of no sliding.

McCallen and Romastad [44] designed an interface element to model the interaction between foundation and the soil. The material nonlinearity of the soil and the components of the building were considered. Since the soil is unable to support a tensile stress, a geometrical nonlinearity exists for uplifting. The geometric nonlinearity of the tall building due to large transverse deflections and the separation between the foundation and soil were studied in [44].

3.3.4 BEM in the linear soil-structure interaction

The BEM involves Green's function for the boundary integral equation [13]. By applying the BEM to the unbounded media, it avoids the time consuming implementation of appropriate border elements and finding the necessary finiteness of mass. The Hankel transform of the Navier's equations in each layer is used to determine the impedance of a rigid, surface or embedded circular foundation. The continuity of the stress vector and displacement at a given interface is satisfied with the help of transmission and reflection coefficients. Extensive calculations which are required for obtaining Green's function and Hankel transformation are the limitations for these methods.

3.3.5 The FE-BE coupling method

The FE-BE coupling method for SSI has been developed by Karabalis and Beskos [33], Spyrakos and Beskos, [64], and Fukui [17]. In later papers ([72] and [73]) the structure was modeled as a linear elastic solid using FEM and the halfspace was modeled as a homogeneous linear elastic solid using BEM. To satisfy the wave radiation condition, transmitting boundaries were developed ([34], [35], [74], and [80]).

In another study [2], the Fourier transformation was used to transform the equation of motion from the time domain into the frequency domain for analyzing transient analysis of dynamic soil-structure interaction. In a free field, the displacement is composed of the incident wave, the reflected wave and the scattered wave. In solving the equations describing the scattered wave, the Hankel function and Green's function were used. The displacement and traction along the interface were obtained. The coupling between FE and BE is accomplished by invoking the traction and displace-

ment continuity across the interface boundary. The displacement and traction are discontinuous at some portion of the interface.

The limitation in BEM is that only a linearly elastic homogeneous domain can be treated. The structure and a small portion of the supporting soil are discretized by FEM, the rest by BEM. This method ignores the rigid foundation and soft soil contact. Consequently, this type of technique avoids this complex interaction.

3.3.6 Kinematics soil-structure interaction effects

Due to input soil motion in an oblique direction instead of a vertical direction, a rigid foundation can not accommodate the variability of the motion of the soil [56]. The foundation will average out the variable input motion and subject the structure to the average motion of the foundation. The averaging process depends on the size of the foundation in depth along the direction of the wave traveling, and also the wave velocity. Some complex methods using the radiating or transmitting boundaries in FEM can take the radiation condition into account. If the foundation is very rigid compared with the adjacent soil, a rocking motion may appear. The rocking and sliding alters the characteristics of the free field motion. Usually, under the assumption that the foundation is rigidly connected to the adjacent soil, the free field motion is applied to the foundation, or on the shared nodes of interface.

3.3.7 Soil-structure interaction and torsional coupling

The torsional response coupled with the SSI for an asymmetrical building was obtained by using an efficient modal analysis [89]. This method allows a more realistic modeling of the building. However, this torsional coupling makes it much more complex in modeling the SSI effects.

Chapter 4

Fundamental Theories of SBFEM and Numerical Development

Several methods can be used to approximate and model the SSI system and different solutions have been achieved with different levels of accuracy. In the past two decades, several novel numerical methods have been developed, including the SBFEM [63] and some hybrid methods ([57] and [45]). All of these methods can be classified into two main categories: the direct method and the substructure method.

In the direct method, the structure and a finite, bounded soil zone adjacent to the structure (near-field) are modeled by the standard FEM and the effect of the surrounding unbounded soil (far-field) is analyzed approximately by imposing transmitting boundaries along the near-field/far-field interface. Many kinds of transmitting boundaries have been developed to satisfy the radiation condition, such as a viscous boundary [43], a superposition boundary [61], and several others [39].

The substructure method is more complex than the direct method in modeling the SSI system. In the substructure method, the soil-structure system is divided into two substructures: a structure, which may include a portion of soils or soils with an irregular boundary, and the unbounded soil ([80] and [81]). These substructures are connected by the general soil-structure interface, as shown in Figure 4.1.

Usually a dynamic soil-structure interaction analysis by the substructure method can be performed in three steps as follows:

(1) Determination of seismic free-field input motion along the general soil-structure interface.

(2) Determination of the reaction of the unbounded soil on the general soil-structure

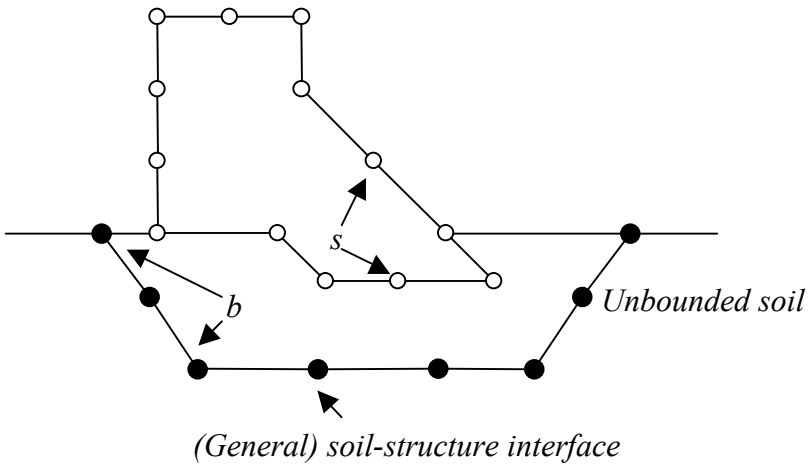

Fig. 4.1: General Soil-Structure Interaction System. s denotes the structure nodes and b denotes the soil-structure interface nodes

interface in the form of a force-displacement relationship.
(3) Analysis of the bounded soil-structure system under the action of the externally applied transient loading and the ground interaction force determined by steps 1 and 2.

The reaction of the unbounded soil on the general soil-structure interface is represented by a boundary condition in the form of force-displacement relationship, which is global in both space and time. The BEM is a powerful procedure for modeling the semi-infinite medium since only the interface of the semi-infinite medium is discretized so that the spatial dimension is reduced by one, and the radiation condition is satisfied automatically as a part of the fundamental solution. Based on the substructure method, many hybrid methods (coupling methods) have been developed where the structure and an adjacent finite region of the soil are discretized by the standard FEM while the unbounded soil is modeled by the BEM. However, it is very difficult to derive the fundamental solutions for many cases. The SBFEM [63] is the alias of the consistent infinitesimal finite-element cell method [88]. It combines the advantages of the BEM and FEM. It is exact in the radial direction, converges to the exact solution in the finite-element sense in the circumferential direction, and is rigorous in both space and time.

The Three-Dimensional Dynamic Soil-Structure Interaction procedure (DSSIA-3D) ([94] and [77]) uses the SBFEM to model the unbounded soil while the structure is modeled using standard FEM. In this numerical procedure, approximations in both time and space, which lead to efficient schemes for the calculation of the acceleration unit-impulse response matrix, are implemented in the SBFEM resulting in an order of magnitude reduction in the required computational effort when compared to other methods. Mathematical details of DSSIA-3D can be found in [94].

4.1 DSSIA-3D

The DSSIA-3D program [94] is a solver for the 3-dimensional dynamic soil-structure interaction problem. A commercial software is used to complete the modeling and discretization. Further detailed information about the input data format can be found in the DSSIA-3D Manual [93]. In oder to apply DSSIA-3D to tall buildings, the solver is updated with an increased capability for large size model with detailed features. The output from the solver is visualized during the post analysis stage. According to

different demands of the design, the free vibration analysis in the frequency domain or the dynamic response in the time domain can be assigned by setting a control variable in the control line of the input data. By using the FFT, the dynamic relationship can be represented as an eigenvalue problem in the frequency domain. After solving this eigenvalue problem, the fundamental frequency, vibration mode, and damping ratio are obtained.

The solving of the eigenvalue program is accomplished by LAPACK, which is a linear algebra library available online. LAPACK is the acronym for Linear Algebra PACKage. It is written in Fortran 77. The LAPACK routines do computations by calling routines in the Basic Linear Algebra Subprograms (BLAS). The LAPACK routines are based in the Level 3 BLAS which provide matrix multiplication. The LAPACK provides either single or double precision. In DSSIA-3D, the double precision is used.

Chapter 5

Dynamic Wave-Soil-Structure Interaction Analysis of Symmetrical Tall Buildings in the Time Domain

This part of research was published in the paper [78], in which DSSIA-3D was applied to obtain the dynamic response of various tall buildings, with multi-level basements, which were subjected to seismic waves. The vibration response of tall buildings to large seismic motions is of great interest to the research community. The literature on this subject contains numerical results using the direct method [68]. Because the direct method is employed, results obtained in that study neglect the effect of the adjacent soil on the amplitude of the motion of the structure and damping ratio of the soil, which is an important factor. Also, in order to achieve the proper accuracy and reduce the effects of reflected waves by the transmitting boundary, it is necessary to consider a large amount of soil around the structure when the direct method is employed. Consequently, the application of DSSIA-3D is extremely advantageous for this problem because this numerical procedure can account for the soil-structure interaction effects, and also the computational effort is significantly reduced. Input P, SH, and SV waves based on the Tabas earthquake recording (Iran, 1978), which is also used in the study by Tehranizadeh [68], are considered.

5.1 Governing equations

If both seismic excitation and externally applied transient loading are considered, the equation of motion of the structure in the time domain can be expressed as [77]:

$$\begin{bmatrix} M_{ss} & M_{sb} \\ M_{bs} & M_{bb} \end{bmatrix} \begin{Bmatrix} \ddot{u}_s^t \\ \ddot{u}_b^t \end{Bmatrix} + \begin{bmatrix} C_{ss} & C_{sb} \\ C_{bs} & C_{bb} \end{bmatrix} \begin{Bmatrix} \dot{u}_s^t \\ \dot{u}_b^t \end{Bmatrix} + \begin{bmatrix} K_{ss} & K_{sb} \\ K_{bs} & K_{bb} \end{bmatrix} \begin{Bmatrix} u_s^t \\ u_b^t \end{Bmatrix} = \begin{Bmatrix} 0 \\ -r_b(t) \end{Bmatrix} + \begin{Bmatrix} p_s(t) \\ p_b(t) \end{Bmatrix} \tag{5.1}$$

where M is the mass matrix, K is the stiffness matrix, u, $\dot{u}$ and $\ddot{u}$ are the displacement, velocity and acceleration vectors, respectively, $r_b(t)$ is the ground interaction force vector, and $p(t)$ are externally applied force vectors. In (5.1), the subscript b denotes the nodes on the soil-structure interface and the subscript s denotes the nodes of the building, as shown in Figure 4.1. The superscript t indicates that the motion of the structure or soil is the total motion. The damping matrix C represents viscous damping matrix. Here, we consider structures subjected to seismic waves only, and consequently external forces on the structure, $p(t)$, are set equal to zero. After the ground interaction force vector, $r_b(t)$, is determined, the dynamic response of the structure can be obtained from (5.1) by using direct integration.

5.2 Ground interaction force

In the substructure method, the ground interaction forces are given by the convolution integral [94]

$$r_b(t) = \int_0^t M_{bb}^g(t-\tau)(\ddot{u}_b^t(\tau) - \ddot{u}_b^g(\tau))d\tau \tag{5.2}$$

where the superscript g represents the unbounded ground soil with excavation, $M_{bb}^g(t)$ is the acceleration unit-impulse matrix, and $\ddot{u}_b^t(t)$ is the acceleration vector at the nodes b (which subsequently lie on the soil-structure interface) of the soil with the excavation. Equation (5.2) can be used to calculate a general wave pattern consisting of body waves and surface waves. The ground motion $\ddot{u}_b^g(t)$ is replaced by the free-field motion $\ddot{u}_b^f(t)$, with the exception of the location of the nodes for which it is to be calculated by the free-field site analysis as shown in [81] and [14]. The free-field system results when the excavated part of the soil is added back to the soil with excavation as indicated in Figure 4.1. For this special case, the structure consists of the excavated part of the soil only, and part of the integral on the right-hand side of

(5.2) can be reformulated by considering the equation of motion as [94]:

$$\int_0^t M_{bb}^g(t-\tau)\ddot{u}_b^g(\tau)d\tau = \int_0^t M_{bb}^f(t-\tau)\ddot{u}_b^f(\tau)d\tau \tag{5.3}$$

where M_{bb}^f is the acceleration unit-impulse response matrix of the free field referred to the nodes at the soil-structure interface. To calculate the acceleration unit-impulse response matrix of the free field, the excavated part of the soil is discretized by the FEM. Standard finite-element discretization of the excavated part of the soil results in the acceleration unit-impulse response matrix M^e of the excavated soil, which is given by

$$M^e = -\frac{1+2\xi i}{\omega^2}K_e + M_e \tag{5.4}$$

where K_e is the stiffness matrix of the excavated soil, M_e the mass matrix, ω the circular frequency, and ξ the hysteretic damping ratio. The matrix M^e can be decomposed into the sub-matrices M_{ii}, M_{ib} and M_{bb}. The subscript b refers to the nodes on the soil-structure interface, and the subscript i refers to the remaining nodes. Eliminating the degree of freedom at the ith node leads to

$$M_{bb}^e = M_{bb} - M_{bi}M_{ii}^{-1}M_{ib} \tag{5.5}$$

where M_{bb}^e denotes the acceleration unit-impulse response matrix of the excavated soil referred to the nodes b. Adding M_{bb}^e to M_{bb}^g results in the acceleration unit-impulse response matrix of the continuous soil (free-field site, refer to Figure 4.1) M_{bb}^f, discretized at the same nodes b, which subsequently lie on the structure-soil interface. That is

$$M_{bb}^f = M_{bb}^e + M_{bb}^g \quad . \tag{5.6}$$

Substituting equations (5.6) and (5.3) into (5.2) gives

$$r_b(t) = r_b^{(1)}(t) + r_b^{(2)}(t) \tag{5.7}$$

where

$$r_b^{(1)}(t) = \int_0^t (t-\tau)(\ddot{u}_b^t(\tau) - \ddot{u}_b^f(\tau))d\tau$$

$$r_b^{(2)}(t) = -\int_0^t M_{bb}^e(t-\tau)\ddot{u}_b^f(\tau)d\tau \quad .$$

The acceleration unit-impulse response matrix $M_{bb}^g(t)$ is calculated using the SBFEM. It may be shown that

$$r_b^{(2)}(t) = -F^{-1}[M_{bb}^e(\omega)\ddot{u}_b^f(\omega)] \tag{5.8}$$

where $F^{-1}[*]$ denotes the Inverse Fourier Transform. The term enclosed in square brackets on the right-hand side of (5.8) is evaluated in the frequency domain and then transformed to the time domain as indicated.

Substituting (5.7) into the equation of motion of structure (5.1) enables the response of this soil-structure system to the incident seismic waves to be determined by a numerical integration scheme in the time domain [94].

5.3 Numerical model

In order to obtain the deformation of the building in an earthquake simulation, the superstructure model is simplified with uniform properties in each cross-section and along the height of the building. The resulting model of the SSI system is composed of one three-dimensional column and the discrete boundary around the basement levels. By using the numerical method to investigate the response of the building, the conceptual overall deformations of the tall building by severe ground motion are obtained.

In an actual experiment by using a test table to simulate the ground motion, the input motion is usually along two orthogonal horizontal directions and one vertical direction in the acceleration-time history data. In this numerical study, the scheme is to assign the input body wave with an angle measured from the horizontal ground plane, in order to simulate the wave propagation in the ground. In the surface wave case, such as a Rayleigh or Love wave, harmonic motion is used. Because the surface waves can result in the most devastating building destruction, it is important to study the effects of these waves on the structures.

5.3.1 Substructure method and direct method

The substructure method, which is employed in the SBFEM, can reduce the number of the degrees of freedom by orders of magnitude when compared to the direct method. In a direct method, modeling of a significant part of soil is essential for accounting for the radiation condition for an unbounded medium. The distance between the artificial soil boundary and the building is usually several times the width of the structure. In a finite-element mesh, the soil will dominate the total number of nodes of the soil-structure system. Therefore, the direct method is usually used to study two-dimensional models only. For a three-dimensional case, the direct method is far less efficient than substructure method. In the substructure method, a layer of the soil around the building's foundation represents the soil domain. A force-displacement relationship is formulated by constructing a unit-impulse response matrix of the unbounded soil. The unbounded soil is modeled by using this analytical result. Consequently, the most number of degrees of freedom are generated in modeling the building structure, instead of the soil. Furthermore, the standard FEM is used to model the tall building because of its advantages of accuracy and convenient standard algorithms in the public domain.

5.3.2 Building model

In order to obtain the deformation of a building in an earthquake simulation, a symmetrical building is simplified with uniform properties along its height. The tall building model is designed with 30 stories above the ground with a 5-story basement as shown in Figure 5.1.

Each story is 18 x 18 x 3.5 m^3 and is divided into 8-node brick elements, 4.5 x 4.5 x 3.5 m^3. Then, each level has 16 brick elements. The number of the total elements for the 35-level building is 560. Each node of the 8-node brick element has 3 degrees of freedom for translational movement referred to a rectangular Cartesian coordinate system. The interface element is a 4-node plate element with each node coincident with one of the structure's element. The SSI interface can be divided into several parts for modeling the soil layers. In this model, only one layer of soil is modeled. There are a total of 112 plate elements and 560 brick elements, and the total nodes are 900. The dynamic stiffness matrix has 2700 degrees of freedom.

5.3.3 Cartesian coordinate system

The origin of the Cartesian coordinate system is assigned to be at the center of the first level, where the building's centerline intersects the ground surface. The Z-axis is pointing downward into the half-space. The X-Y plane is the ground surface. The building is symmetrical about the coordinate planes, X-Z and Y-Z. We select the X-Z plane as the input plane for the input ray. The input angle is measured from the positive X-axis to the direction of the wave propagation, as shown in Figure 5.2. In this study, a seismic recording is input at the origin of the coordinate system, which is the control point.

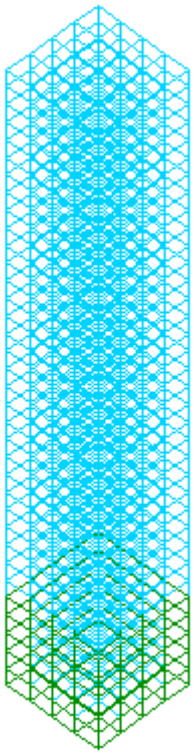

Fig. 5.1: A finite-element model of a 30-story building with a 5-level basement. The green represents the adjacent soil layer. The soil layer is modeled by using the scaled boundary finite-elements which share the same plate element of the structure. The blue elements are the structural brick elements.

5.3.4 Soil properties

Soil properties are assigned to the nodes on the interface with the building. In this study, the displacement of the buildings at the ground level is of the most interest.

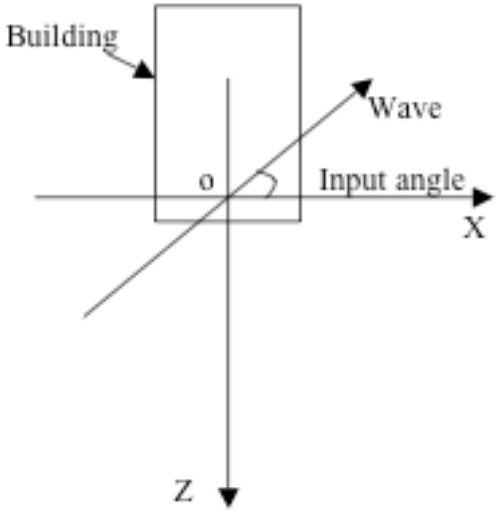

Fig. 5.2: The coordinate system.

The dynamic response of the buildings depends on the soil properties and damping ratios of the soil and buildings. The soil properties will be given in a following section.

5.4 Numerical results

The first example investigates the response of a 30-story building, with a 5-level basement, subjected to P, SH, and SV waves at incident angle of 90, 60, and 30 degrees measured from the horizontal direction. The displacements of each story are compared between different cases with different input angles for one input wave type and with different wave types.

When using a shaking table to simulate the ground motion, the input motion is given along two orthogonal horizontal directions and one vertical direction. However, in this numerical example, the scheme is to assign the input body wave with an angle measured from the horizontal direction to the propagation direction, which simulates real wave motion in the unbounded soil. In both methods, the acceleration-time history data is used as the input signal.

In order to obtain the response of various tall buildings subjected to identical seismic recordings, 5-, 10-, 20- and 30-story buildings are modeled and simulated, each with 5-level basements. The 5-, 10-, 20-, and 30-story buildings are noted as model A, B, C and D, respectively.

The amplitudes of the displacements along the height of the other three buildings are compared with the 30-story building, subjected to same input motion. The influence of the configuration of the building on the vibration and deformation are obtained.

The peak displacements (PD) of the building during vibration are recorded and used to analyze the dynamic behaviours of the tall buildings subjected to earthquakes. The difference between PD and the displacement at any time interval is that the PD represents the largest displacement that occurred during that time interval. The displacements of the nodes are relative to the static position before the input of the seismic waves.

5.4.1 Non-dimensionalization scheme

Here, a non-dimensional scheme is used. The story height H and shear wave velocity c_s in the soil are used as the characteristic length and velocity, respectively. The

characteristic time is represented as:

$$\hat{t} = \frac{H}{c_s} \quad .$$

Therefore,

$$\bar{t} = \frac{t}{\hat{t}}, \quad \bar{u} = \frac{u}{H}, \quad \bar{c_p} = \frac{c_p}{c_s}, \quad \bar{c_s} = 1, \quad \bar{E_b} = \frac{E_b}{E_s}, \quad \bar{E_s} = 1, \quad \bar{\rho_b} = \frac{\rho_b}{\rho_s}, \quad \bar{\rho_s} = 1$$

are non-dimensional time, displacement, P-wave velocity, S-wave velocity, and Young's modulus and densities of the building and soil, respectively. The story height H is 3.5 m. The shear wave velocity c_s is 774 m/s and dilatational wave velocity c_p is 1,341 m/s. The density of the reinforced concrete ρ_b is 2,500 kg/m^3, and the density of the dense soil ρ_s is 2,000 kg/m^3. Young's modulus of the reinforced concrete building E_b is 30 GPa. Henceforth, the superposed bar will be omitted.

5.4.2 Case study for a 30-story building

P waves

When a P wave is input vertically (measured 90 degrees from the horizontal), the largest deformation occurs in the vertical axis direction, as shown in Figure 5.3. During a strong earthquake (Tabas, 1978), the basement level endures the greatest displacement. The displacement dramatically changes around the surface. The dilatational wave transfers the energy through the stress generated in the building, after the foundation is stressed by the vertically input wave. Because the model is symmetrical, the horizontal displacement in the X and Y directions are largely of the same fashion. The horizontal displacement amplitude is relatively small compared with the deformation in the vertical direction. When the earthquake wave input angle changes from 60 to 30 degree, there is a larger horizontal component of motion transferred to the superstructure, as shown in Figures 5.3-5.5. The X direction amplitude of the displacement of the node in the centerline of the building becomes the dominant vibration component. This type of large continuously horizontal vibrations may damage the structure. Therefore, the shear strength of the structure is a very important factor for resisting earthquakes. The PD along the X direction increases to the same order of magnitude as the vertical PD when input angle is 60 degrees; and the X component of motion is even larger at 30 degrees input angle, which is

closer to the horizontal plane. Since the seismic input plane is the X-Z plane, the X direction is influenced more than the Y direction. The energy dissipated by the inter-story drift also increases. When the same intense P wave impacts the building with a smaller input angle, a larger displacement and consequently more damage will be observed. Therefore, the characteristics of deformation and vibration of buildings depend on the earthquake wave input angle for the case of dilatational waves.

Shear waves

The SH wave is a shear wave with the particle motion direction parallel to the ground surface, and perpendicular to the X-Z input plane, as shown in Figure 5.2. For an input angle of 60 degrees, the main component of the displacement occurs in the Y direction. The building absorbs the kinetic energy with large displacements occurring at the ground level. As shown in Figure 5.6, the PD is at a maximum at the ground level, decreases approximately proportional with the height of the building from the ground level to the roof. The X, Z displacements are much smaller components, which can be neglected.

The SV wave is a shear wave with the particle motion perpendicular to the wave travel direction and coincident with the X-Z input plane. In this case, the X, Z components are the main components of the displacement for a wave input angle of 60 degrees. As a result, most of the energy is transferred in the input plane along the X, Z direction. As shown in Figure 5.7, the maximum PD in X direction occurs at the level close to the ground and then rapidly decreases.

5.4.3 SSI analysis

The relationship between the input wave type and the subsequent deformation of the buildings is influenced by the interaction between the soil and foundation. In this model, the unbounded soil is represented by the soil-structure interface and the ground motion is assigned to control points, which simulates the motion due to an earthquake. Thus large deformations of the foundation are expected. The more explicit SSI effects, such as separation occurring between the soil and foundation are not modeled here.

The SSI effect is demonstrated by the distribution of PD obtained in the analysis at the underground level. Because of the interaction between the structure and the adjacent soil, the motion of the soil influences the deformation of the building. Consequently, the peak values of displacement usually occur at the ground level, which

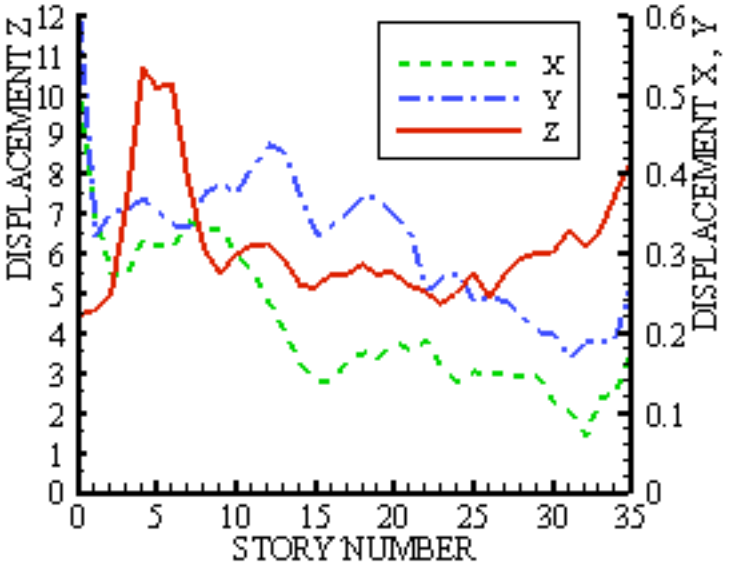

Fig. 5.3: Non-dimensional peak displacement (x10^3) of the centerline of the model D for P wave incident at a vertical angle.

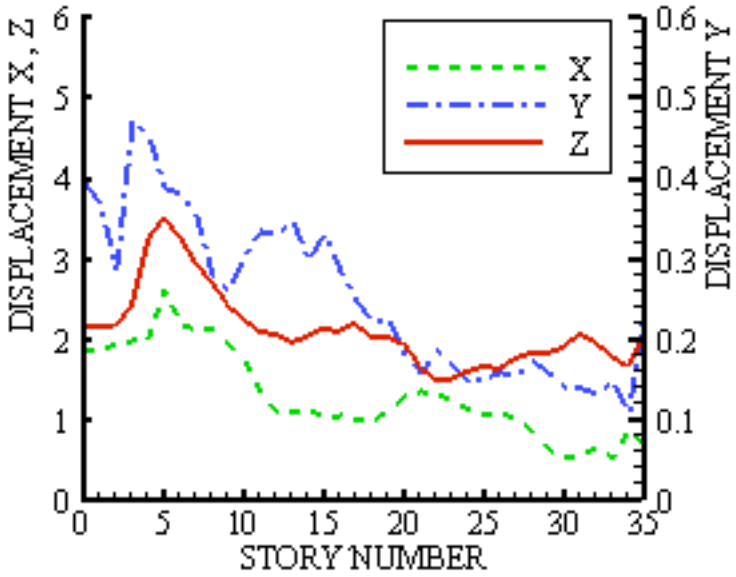

Fig. 5.4: Non-dimensional peak displacement (x10^3) of the centerline of model D for a P wave at 60^o input angle.

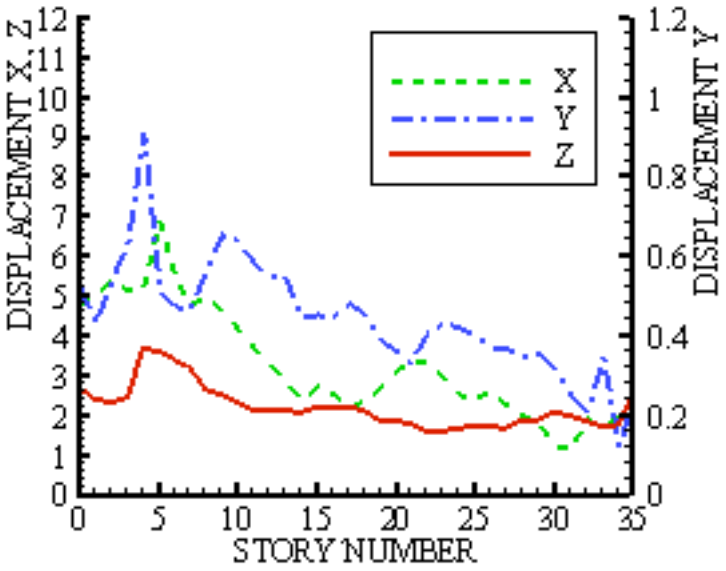

Fig. 5.5: Non-dimensional peak displacement (x10^3) of centerline of model D for a P wave at 30^o input angle.

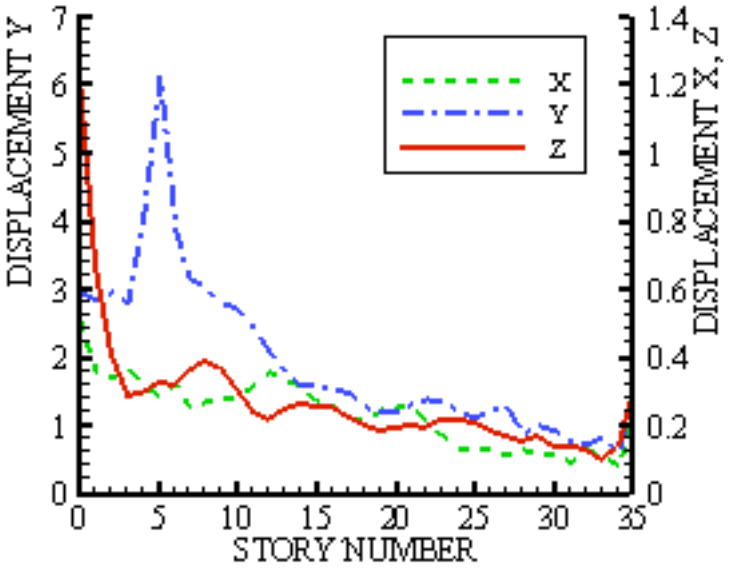

Fig. 5.6: Non-dimensional peak displacement (x10^3) of the centerline of model D for a SH wave at 60^o input angle.

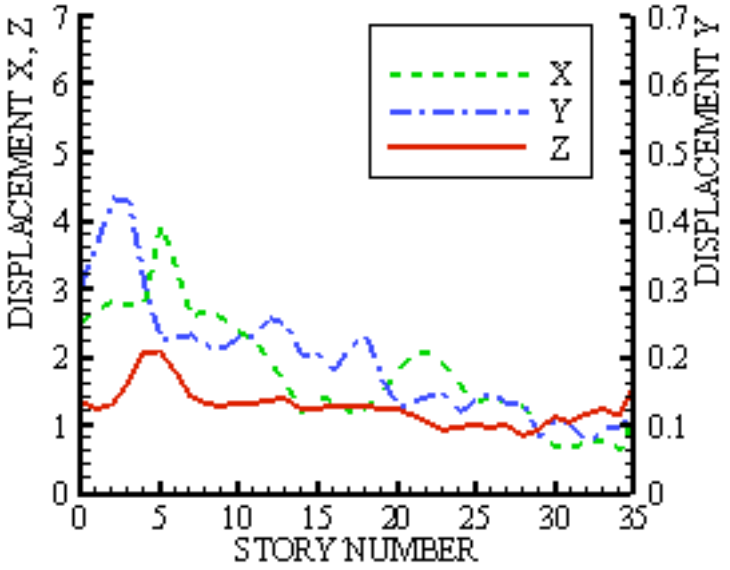

Fig. 5.7: Non-dimensional peak displacement (x10^3) of the centerline of model D for a SV wave at 60^o input angle.

is located between the soil and free surface.

5.4.4 Building height

In order to compare the damage of buildings of different heights, and for different types of input ground motions; a group of four models A, B, C and D, are investigated.

For the P wave, at input angles of 60 degrees and 90 degrees, the buildings of shorter height have larger PD in the vertical direction, as shown in Figures 5.8-5.9. The largest displacements occur for building heights in the range of 5 to 10-stories. By comparing the deformation in X direction, this illustrates that the buildings of shorter height have a greater horizontal oscillation from the original position than do taller buildings.

As shown in Figures 5.10-5.11, for both SH and SV waves, models B, C and D have similar slopes in the peak displacement along the horizontal directions, X or Y, for an input angle of 60 degrees. The model A has the same slope when the input wave is an SH wave. It has a large drift that can be verified from the displacement-time history of the roof center. This study shows the response of buildings with different heights for one earthquake event. The taller building has less inter-story drift at upper levels; consequently the larger inter-story drift at lower heights may be the reason for causing structural failure during strong earthquakes. From field observations, the shorter residential buildings, of four to five stories, are the most vulnerable to earthquakes of large magnitudes.

5.5 Conclusions: SSI in the time-domain analysis for tall buildings

Based on a new numerical procedure for solving problems of wave-soil-structure interaction, we investigated the response of buildings, of four different heights, subjected to earthquakes of large magnitudes. The peak displacement of the nodes on the centerline of the buildings are obtained and compared by considering the SSI effects and building heights. The largest deformation of the buildings occurs at the basement levels, which are close to the ground surface. P waves cause more deformation and movement along the input direction. Shear waves, SH and SV waves, cause much more inter-story drift.

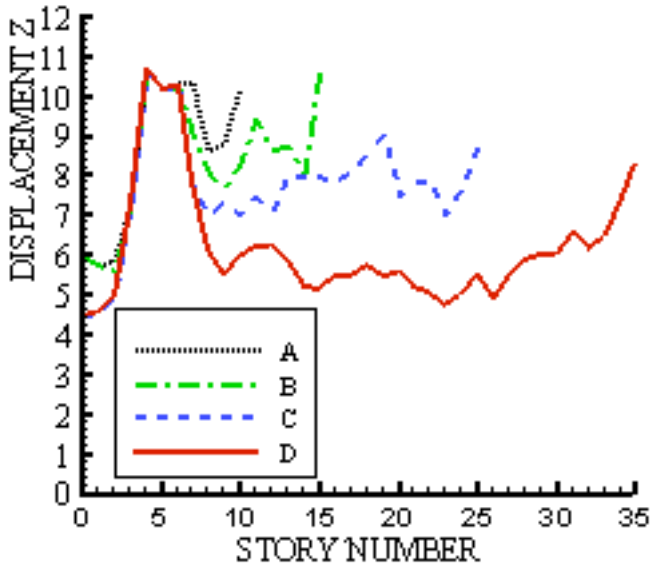

Fig. 5.8: Non-dimensional displacement (x10^3) of nodes in the centerline of models for a P wave incident at a vertical angle.

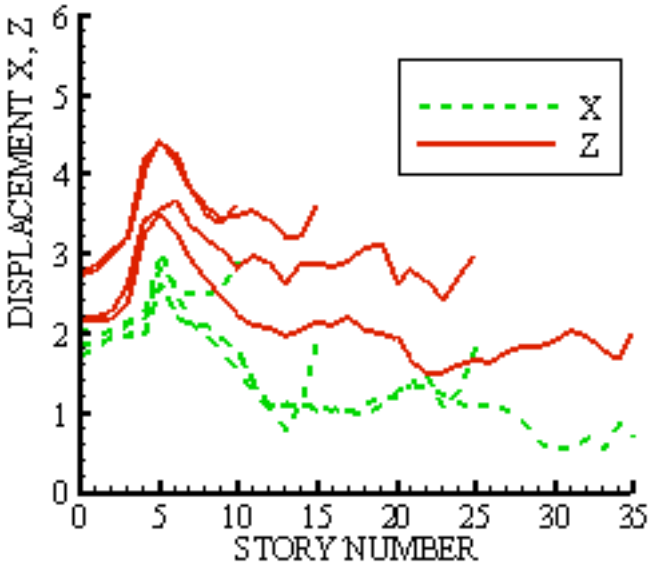

Fig. 5.9: Non-dimensional displacement (x10^3) of nodes in the centerline of models for a P wave at 60^o input angle.

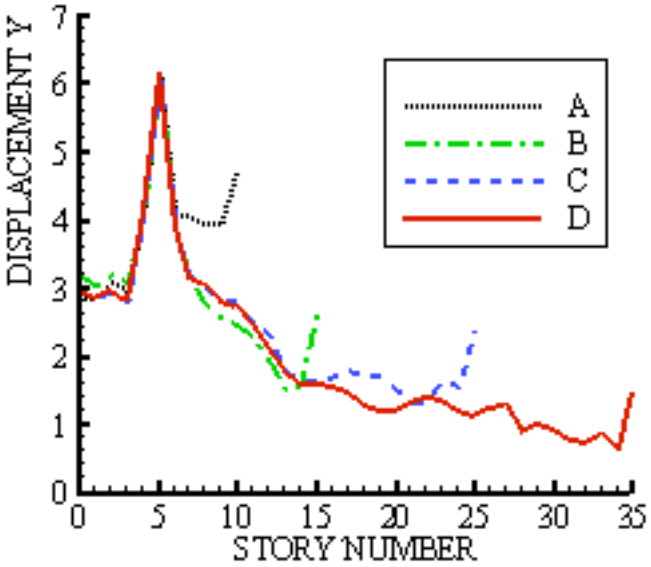

Fig. 5.10: Non-dimensional displacement (x10^3) of nodes in the centerline of models for a SH wave at 60^o input angle.

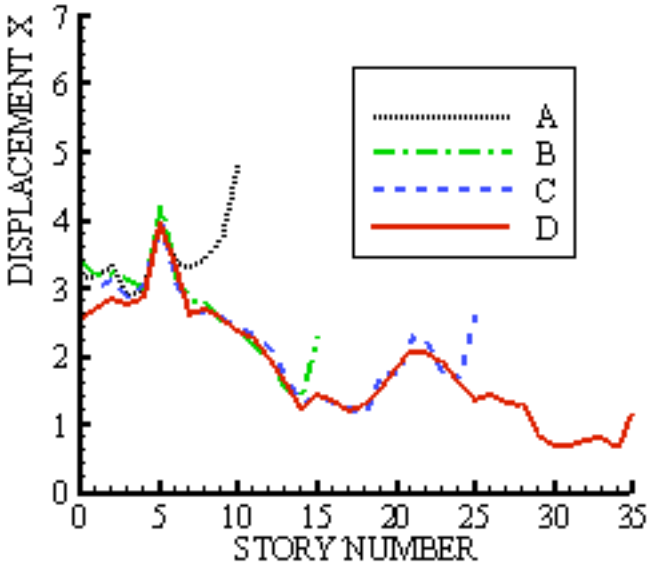

Fig. 5.11: Non-dimensional displacement (x10^3) of node in the centerline of models for a SV wave at 60 degree input angle.

Chapter 6

Dynamic Wave-Soil-Structure Interaction Analysis of Symmetrical Tall Buildings in the Frequency Domain

There are several methods of obtaining the fundamental frequency of a tall building. The natural frequency of the tall building can be estimated by analytical methods ([9] and [27]), numerical methods, experimental methods such as a wind channel test or a shaking table test, or in situ measurement. Among these methods, the analytical methods need ideal assumptions to obtain solutions and therefore there are limitations on using these results. The experimental methods, such as a wind channel test and a shaking table test, are usually expensive and limited by the specific capacity and the scale of the building replica. In the field measurement method, the natural frequencies and the vibration modes are detected from a large amount of field measurements sampled from acceleration sensors and displacement sensors installed on the building, and a typhoon or seismic tremor are used as the input vibration sources [53]. Compared with the above methods, numerical methods, such as the FEM, BEM, and hybrid FE/BE method, give promising means to model the building free vibration with soil-structure interaction and are able to solve this eigenvalue problem with a less cost and better accuracy. Using numerical methods, the fundamental frequency, vibration mode, and associated radiation damping ratio can be obtained.

When a substructure method is applied to a soil-structure system, the dynamic-stiffness matrix is frequency dependent and complex, and the orthogonality condition is not satisfied. Consequently, the equations of motion cannot be uncoupled, and the classical mode-superposition method is not applicable. However, it is of interest in earthquake engineering to investigate the free-vibration frequencies and the corresponding radiation damping ratios, especially for the modes of vibration with the lowest frequencies.

In a substructure method, the effect of the unbounded soil on the structure is represented by a force-displacement relationship and a non-linear eigenvalue problem is obtained for the analysis of the three-dimensional soil-structure system. The SBFEM is used to model the unbounded soil, while the FEM is used to model the structure, as shown in Figure 6.1. Inverse iteration, proposed by [77], is used to solve the non-linear eigenvalue problem. The fundamental frequencies, the corresponding equivalent radiation damping ratios as well as the eigenvectors are obtained for various tall buildings with an one-level basement.

6.1 Governing equations

6.1.1 Equation of motion

Representing the force-displacement relationship in the frequency domain and using similarity theory, as the thickness of the finite-element cell approaches zero, the dynamic stiffness at the exterior boundary converges to the dynamic stiffness at the interior boundary. The force-displacement relationship can be given in frequency domain by

$$r_b(\omega) = \bar{S}^g_{bb}(\omega)(u^t_b(\omega) - u^g_b(\omega)) \tag{6.1}$$

where the subscript b denotes the nodes of the interface, the superscript t denotes the total displacement of the nodes and the superscript g denotes the motion of the ground with excavation as shown in Figure 4.1. In (6.1), the vector $r_b(\omega)$ is the interaction force on the nodes on the soil-structure interface, the matrix $\bar{S}^g_{bb}(\omega)$ is a dynamic-stiffness matrix of the nodes on the soil-structure interface, and $u^t_b(\omega)$ is the displacement vector of the nodes on the soil-structure interface. In this study, the scattered motion of incident waves $u^g_b(\omega)$ is zero. More details of this mathematical model can be found in [77].

For a soil-structure system without an applied force, the equations of motion of the structure in the frequency domain [77] can be expressed as:

$$\begin{bmatrix} S_{ss}(\omega) & S_{sb}(\omega) \\ S_{bs}(\omega) & S_{bb}(\omega) \end{bmatrix} \begin{Bmatrix} u_s^t(\omega) \\ u_b^t(\omega) \end{Bmatrix} = \begin{Bmatrix} 0 \\ -r_b(\omega) \end{Bmatrix} \tag{6.2}$$

where the dynamic matrix of the structure is calculated as:

$$S(\omega) = K(1 + 2\xi_h i) - \omega^2 M \tag{6.3}$$

where ξ_h is the hysteretic damping ratio of the structure, M is the mass matrix, K is the stiffness matrix and the subscript b and s denote the nodes of interface and structure, respectively, as shown in Figure 4.1. The interaction force between the soil and the foundation of the structure is given by (6.1).

6.1.2 Nonlinear eigenvalue problem

Substituting (6.1) into (6.2) results in,

$$\left((1 + 2\xi_h i) \begin{bmatrix} K_{ss} & K_{sb} \\ K_{bs} & K_{bb} + \frac{\bar{S}_{bb}^g(\omega)}{1+2\xi_h i} \end{bmatrix} - \omega^2 \begin{bmatrix} M_{ss} & M_{sb} \\ M_{bs} & M_{bb} \end{bmatrix} \right) \begin{Bmatrix} u_s^t \\ u_b^t \end{Bmatrix} = 0 \quad . \tag{6.4}$$

Equation (6.4) is a non-linear eigenvalue problem. The dynamic-stiffness matrix is frequency-dependent, and hence (6.4) is difficult to solve.

The free vibration frequencies and the corresponding modal shapes can be obtained as the solution of (6.4), but the orthogonality condition is not satisfied for the soil-structure system. Consequently the modal shapes cannot be used to decouple the equations of motion. Free-vibration frequencies and the corresponding radiation damping ratios of the lowest few modes of vibration are of considerable interest in earthquake engineering. It is possible to obtain all free-vibration frequencies and corresponding mode shapes, but the fundamental frequency of a soil-structure system is of the most importance in earthquake engineering. The inverse iteration procedure outlined by [77] is used in this study to evaluate the fundamental frequency, the corresponding radiation damping ratio and mode shape. The complex dynamic-stiffness matrix $\bar{S}_{bb}^g(\omega)$ can be decomposed as:

$$\bar{S}_{bb}^g(\omega) = K_{bb}^g - \omega^2 M_{bb}^g(\omega) \quad , \tag{6.5}$$

where the matrix $K_{bb}^g = \bar{S}_{bb}^g(0)$ is the static stiffness matrix of the unbounded soil and is a real constant matrix. Substituting (6.5) into (6.4) results in

$$[(1+2\xi_h i)K - \omega^2 \bar{M}(\omega)]u^t = 0 \quad , \tag{6.6}$$

where

$$K = \begin{bmatrix} K_{ss} & K_{sb} \\ K_{bs} & K_{bb} + \frac{K_{bb}^g}{1+2\xi_h i} \end{bmatrix}$$

and

$$\bar{M}(\omega) = \begin{bmatrix} M_{ss} & M_{sb} \\ M_{bs} & M_{bb} + M_{bb}^g(\omega) \end{bmatrix} \quad .$$

The inverse iteration solution of (6.6) is formulated by

$$\begin{aligned} u^{t(0)} &= [1,1,...,1]^T \quad , \\ K\bar{u}^{t(j)} &= \bar{M}(\omega^{(j-1)})u^{t(j-1)} \quad , \\ u^{t(j)} &= \frac{\bar{u}^{t(j)}}{max(\bar{u}^{t(j)})} \quad , \\ \lambda^{(j)} &= \frac{(\bar{u}^{t(j)})^T \bar{M}(\omega^{(j-1)})u^{t(j-1)}}{\bar{u}^{t(j)}\bar{M}(\omega^{(j-1)})\bar{u}^{t(j)}} \quad , \\ \omega^{(j)} &= \sqrt{\lambda^{(j)}(1+2\xi_h i)} \quad , \end{aligned} \tag{6.7}$$

where $max(\bar{u}^{t(j)})$ is the largest element of the $\bar{u}^{t(j)}$ and is used to normalize the $\bar{u}^{t(j)}$. In (6.7), the matrix K is a complex constant matrix; therefore it is factored only once throughout the iterations. From (6.7), the fundamental frequency, the corresponding radiation damping ratio and mode shape can be obtained. The free-vibration frequency of the jth mode of vibration obtained from (6.7) can be expressed in the following form:

$$\omega_j = a_j + ib_j \quad , \tag{6.8}$$

where a_j and b_j are the real and imaginary parts of ω_j. The free-vibration of the damped system of the jth mode can be written as:

$$u_j^t(t) = u_j^t(t)\exp(-b_j t + i a_j t) \quad . \tag{6.9}$$

Equation (6.9) represents the free vibration of a damped system. The free-vibration frequency of the damped system of the jth mode of vibration, ω_{D_j} and the corresponding damping ratio, ξ_j can be obtained as:

$$\omega_{D_j} = a_j \quad , \tag{6.10}$$

$$\xi_j = \frac{b_j}{\sqrt{a_j^2 + b_j^2}} \quad , \tag{6.11}$$

respectively.

The hysteretic damping ratio indicates the internal energy loss due to building vibrations, which is included in the general damping ratio ξ_j. If the hysteretic damping ratio of a structure, ξ_h, is equal to zero, the damping ratio obtained from (6.11) is the radiation damping ratio ξ_j only. The radiation damping ratio is the result of the energy loss due to the assumption that the wave is not reflected back and dissipates completely after passing through the boundary. Consider any two positive peaks, u_j^n and u_j^{n+m} which are m cycles apart and occur at times $n(2\pi/a_j)$ and $(n+m)2\pi/a_j$, respectively. Using (6.9), the ratio of these two values is given by

$$\frac{u_j^n}{u_j^{n+m}} = \exp(2\pi m b_j/a_j) \quad . \tag{6.12}$$

The damping ratio, ξ_j, follows from (6.11) and (6.12) as:

$$\xi_j = \frac{\delta}{\sqrt{4\pi^2 m^2 + \delta^2}} \tag{6.13}$$

where $\delta = \ln(u_j^n/u_j^{n+m})$. The above mentioned numerical procedure is largely cited from paper [77].

6.2 Building model

The buildings are assumed to be geometrical symmetrical with uniform properties along the height with a square floor plan. A tall building model designed with 15 stories above the ground, with an one-level basement, is shown in Figure 6.1. For the purpose of analysis, each story is 18 x 18 x $3.5m^3$ and is divided into 4 units

separated by walls. The floor is 40 cm in thickness. The number of the total of 8-node brick elements for the 15-level building is 1824. Each node of the 8-node brick element has 3 degrees of freedom for translational movement in a rectangular Cartesian coordinate system. The 4-node interface element has each node coincident with one of the element of the structure at the basement level. The SSI interface can be divided into several parts for modeling the soil layers. In this model, only one layer of soil is modeled. There are a total of 18 interface elements and 1824 brick elements, and the total nodes are 3300. The dynamic stiffness matrix has 9900 degrees of freedom.

In the past two decades, the research into methods capable of obtaining the free vibration of tall buildings has become of considerable interest, and consequently, there is extensive literature on this subject. However, the limitation of studies currently found in the literature is the exclusion of the effects of the soil-structure interaction. The present study investigates the effects of the SSI on the free vibration of tall buildings, with basements, in three dimensions, which is an improvement over previous investigations. The numerical results obtained in this study are compared to those obtained by Tehranizadeh who used the direct method and is restricted to a two dimensional analysis [68] . Also, the SSI effect is not considered in [68]. The numerical results are also compared to those obtained from the Uniform Building Code (UBC) [71].

6.3 Numerical results

A parametric study is carried out here for investigating the effect of the soil-structure interaction with a group of 5 buildings of 5-, 10-, 15-, 20- and 25-stories, each with a one-level basement. The fundamental frequencies and radiation damping ratios of the soil-structure systems are compared for buildings of various heights, and the soil-structure interaction effect is addressed. First, the relationship between the soil-structure effect and the height of the building is investigated. Then, for a specific case, a 15-story building is chosen to examine further the relationship between the material properties of the soil and the response of the structure. From this case study, the influence of Young's modulus of the soil on the response of the building is addressed. At last, the relationship between the structural hysteretic damping ratio (6.7) and the response of the building is investigated.

The material properties of the soil [68], and the properties of the concrete structure

Fig. 6.1: Finite element model of 15-story building with an one-level basement. The green layer represents soil layer. The soil layer is modeled by using the scaled boundary finite-elements which share the same interface element of the structure. The red elements are the structural brick elements.

[20] are given in Table 1.

The disadvantage of the direct method used by Tehranizadeh [68] is that a significant mass of soil must be modeled around the structure, which usually makes large demands on computational storage. Therefore, this method is restricted to a two-dimensional analysis. The method presented here is a three-dimensional analysis and results can be obtained on a PC.

Table 6.1: The properties of the adjacent soil and reinforced concrete structure

Material	E (MPa)	ν	ρ (Kg/m^3)	Damping Ratio
Soil	36.4 ∼1101.1	0.3	1400	0.0
Reinforced Concrete	30000	0.2	2500	0.1

Note: where the E is the Young's modulus, ν is the Poisson's ratio and the ρ is the density. The damping ratio here is the hysteretic damping ratio. We assume the soil has no hysteretic damping ratio and the building structure has a hysteretic damping ratio of 0.1.

6.3.1 Building height

The fundamental frequencies for structures with zero hysteretic damping ratio for one group of models with one-level basement are shown in Figure 6.2. The corresponding fundamental frequencies calculated from the Uniform Building Code [71] are also shown for comparison in Figure 6.2. It is important to note that the results obtained from the Uniform Building Code do not include the SSI effect, which is included in the inverse iteration procedure used in this study to obtain numerical results. In Figure 6.2, an examination of the fundamental frequency distribution shows that discrepancies exist between the numerical results and those obtained using the Uniform Building Code formula, especially for those buildings of lower height. The fundamental frequencies for the Uniform Building Code are consistently lower than those obtained numerically. However, as the height of the building increases, this discrepancy decreases.

This discrepancy can be explained by noting that the Uniform Building Code [71] is a simplified empirical formula which calculates the fundamental frequency of a structure based on the height and material of a structure.

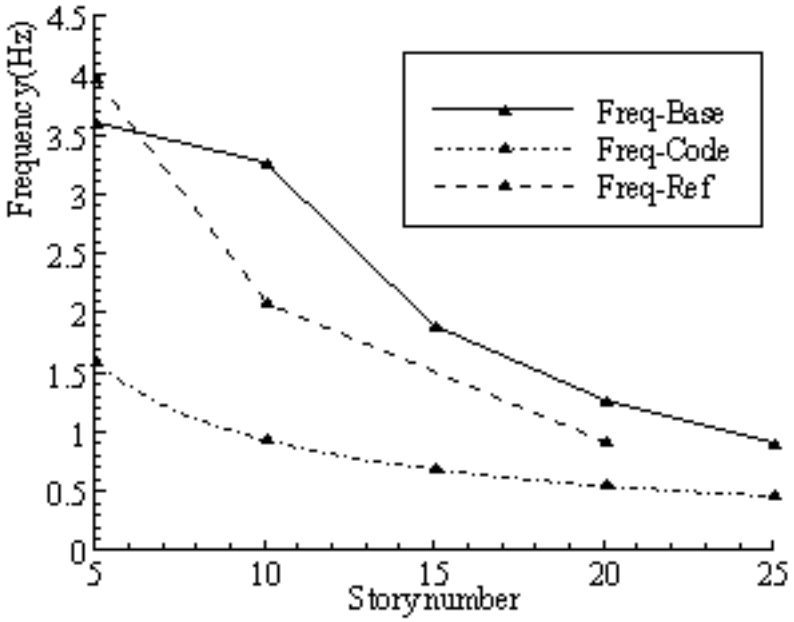

Fig. 6.2: Fundamental frequency: the term (-Base) refers to a building with basement levels; the term (-Code) refers to the calculations from UBC [71]; the term (-Ref) refers to the results of Tehranizadeh [68].

6.3.2 Soil-structure interaction effect

In order to study the influence of the properties of the soil on the response of a tall building, a 15-story building with a one-level basement is chosen for a detailed investigation. The distribution of the fundamental frequency of the building with Young's modulus (with units of MPa) of the soil is shown in Figure 6.3. For different types of soil, the density is assumed as constant at 1,400 kg/m^3. The soil stiffness ranges from 36.4 MPa to 1,101.1MPa and correspondingly, the shear wave velocity ranges from 100 m/s to 550 m/s. As shown in both figures, the fundamental frequency monotonically increases with the stiffness of the soil as expected.

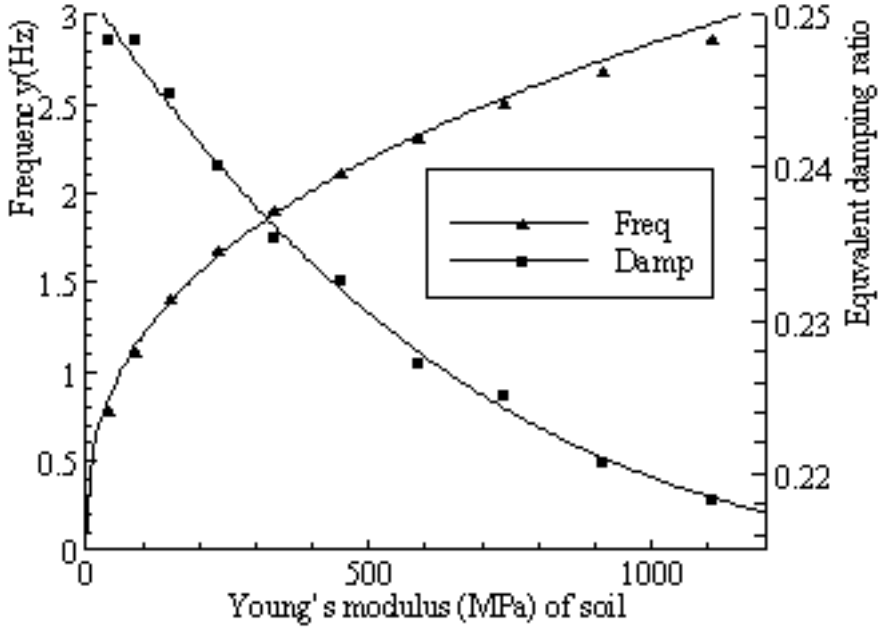

Fig. 6.3: Fundamental frequency and equivalent damping ratio of 15-story building with an one-level basement.

6.3.3 Hysteretic damping ratio

When a building vibrates, there may be a loss in structural integrity such as the failure of weld joints and crack development of concrete frames. The hysteretic damping ratio would increase under these conditions. Therefore, in this study, the hysteretic damping ratio of the building is varied from the assumed value of 0.1. As shown in Figure 6.4, for a 15-story building, when the hysteretic damping ratio increases from 0.1 to 0.4, the fundamental frequency increases slightly from 2.122Hz to 2.181Hz. The

hysteretic damping ratio of 0.4 is unrealistic for most structures, however we use it here for illustrative purposes.

As the hysteretic damping ratio increases, the equivalent damping ratio (6.11) also increases. From the solutions of the eigenvalue problem, the damping ratio obtained from equation (6.11) includes the hysteretic damping ratio of the structure in addition to the radiation damping ratio and therefore, the damping ratio obtained from equation (6.11) is an equivalent ratio instead of the radiation damping ratio. Consequently, as the hysteretic damping ratio increases, the damping ratio obtained from equation (6.11) also increases. For a high-rise building, in addition to the specification of the site soil and structure properties, the hysteretic damping ratio also influences the energy dissipation mechanism between the SSI system and unbounded soil.

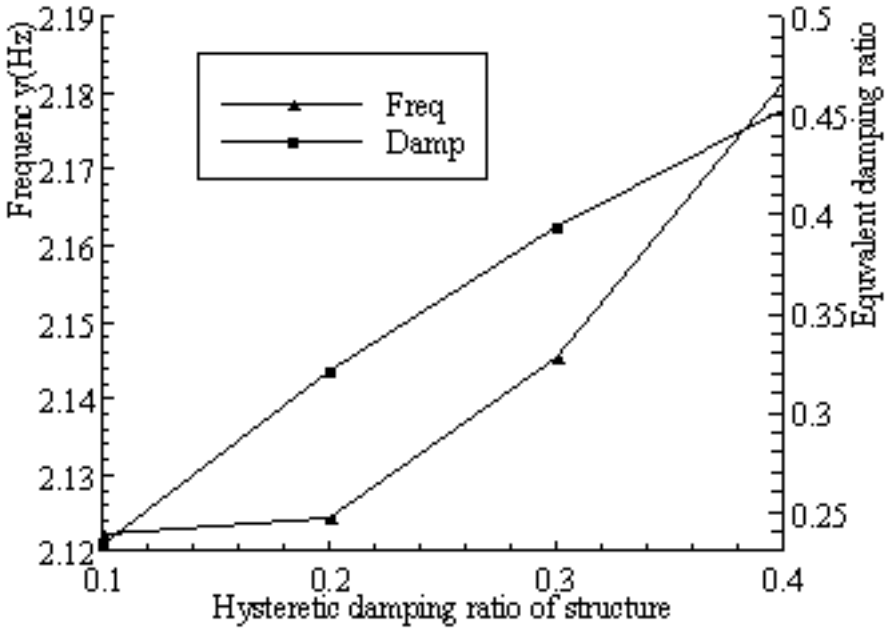

Fig. 6.4: Hysteretic damping ratio and fundamental frequency of 15-story building with an one-level basement. The other material properties from those given in Table 6.1 are assumed unchanged.

6.4 Concluding remarks on frequency domain analysis of tall buildings

Owing to the frequency dependence of the radiation damping, the orthogonality condition for the modes is not satisfied for the soil-structure system considered in this study. Hence the classic mode-superposition method is not applicable to soil-structure system. However, it is of interest in earthquake engineering to evaluate the fundamental frequency, and the corresponding damping ratio.

The hysteretic damping ratio of the structure influences the fundamental frequency and the equivalent radiation damping ratio. Furthermore, the fundamental frequency of the building characterizes the response of the soil-structure system; and the associated damping ratio corresponds to the energy dissipation of the soil-structure system to the unbounded soil.

The limitations of this procedure are that currently it is restricted to linear problems because it is based on the boundary element method. However, it can be modified by incorporating a meshless method in the near-field around the structure to include nonlinearities.

The results here contribute to the understanding of the soil-structure interaction effect and consequently will greatly improve the design process by either including seismic resistance properties in the initial design of buildings or allowing accurate seismic upgrades to existing buildings.

Chapter 7

Dynamic Wave-Soil-Structure Interaction Analysis of Two-way Asymmetrical Tall Buildings

Asymmetrical buildings are more vulnerable to earthquake hazards than buildings with a symmetrical configuration. The recognition of this sensitivity has led researchers to concentrate their studies on earthquake characteristics, evaluation of the structural parameters and validity of the system models ([29], [30], [24], [12], [58], [46], [60]). So far, several researchers have attempted to evaluate the seismic response behaviour of torsionally coupled buildings for the linear analysis of three dimensional dynamic soil-structure interactions of asymmetrical buildings [3]. The influence of dynamic soil- structure interaction on seismic response is studied in [59], selecting a set of reinforced concrete structures with gravitational loads and representative systems designed for earthquake resistance in accordance with current criteria and methods.

7.1 Two-way asymmetrical building model

In past years, the seismic response of asymmetrical structures has been frequently analyzed by means of single story models, because of their simplicity and low computational cost. In this study, a two-way asymmetrical 15-story building with one level basement model, as shown in Figures 7.1 and 7.2, is studied. The dimensions of the floor are 18 x 18 x $0.40m^3$, the height between floor and ceiling is 3.10 m and the thickness of wall is 20 cm. Each floor is divided into 4 units separated by

walls and the material used for the building is concrete. The wall and floor of this super-structure are meshed into 1872 8-node brick elements with 3 DOFs for each node. There are 1534-node interface elements along the soil-structure interface. The excavated soil is meshed into 162 brick elements at the basement. The total nodal nodes of this building model are 3300. The origin of the Cartesian coordinate system at the center of the first level, where the centerline intersects the ground surface, as shown in Figure 7.4. The Z-axis is pointing downward into the half-space. The X-Y plane is the ground surface. The geometry of the building is symmetrical about the coordinate planes, X-Z and Y-Z. We select the X-Z plane as the input plane without loss of the generalization. Here the angle of incidence is not used. Instead, its complement measured from the positive X-axis to the direction of the wave propagation is used.

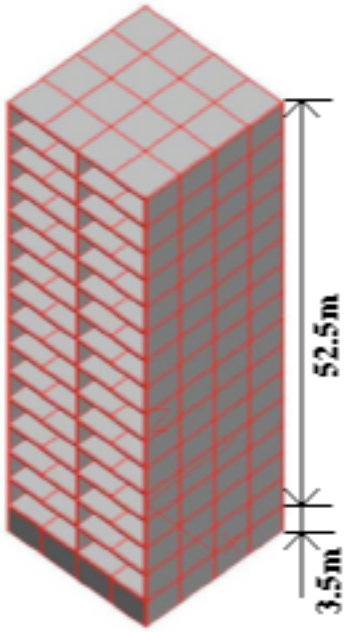

Fig. 7.1: The architecture model

In this study, a seismic recording is input at the origin of the coordinate system, which is the control point. Only mass asymmetry is considered. The mass eccentricity is achieved by adjusting the mass density of the floor. The eccentricity of the building is large and mass center is located away from the geometrical center in the first quadrant. The eccentricity may be caused by the uneven mass distribution on the floor, such as equipment. In reality, the eccentricity is the result of the asymmetrical

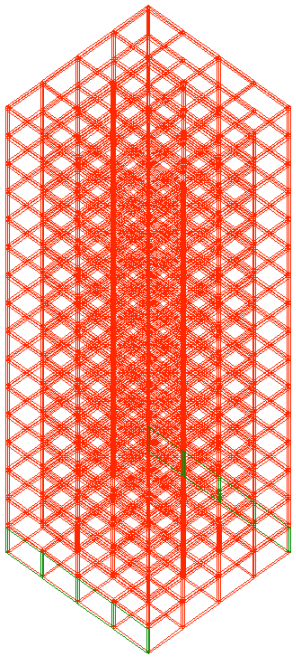

Fig. 7.2: The finite-element mesh model

configuration of a building, such as an "L" shape building. However, here we focus on the mass eccentricity only. The finite-element mesh, its architecture configuration and floor dimensions are given in Figures 7.1-7.3. The nodal points along the interface between soil and the building are given the soil properties, such as the density, Young's modulus and Poisson's ratio.

In this study, the displacement of the building at the ground level is of most interest. The dynamic response of the building depends on the soil properties and on both the damping ratio and stiffness ratio of the soil and the building.

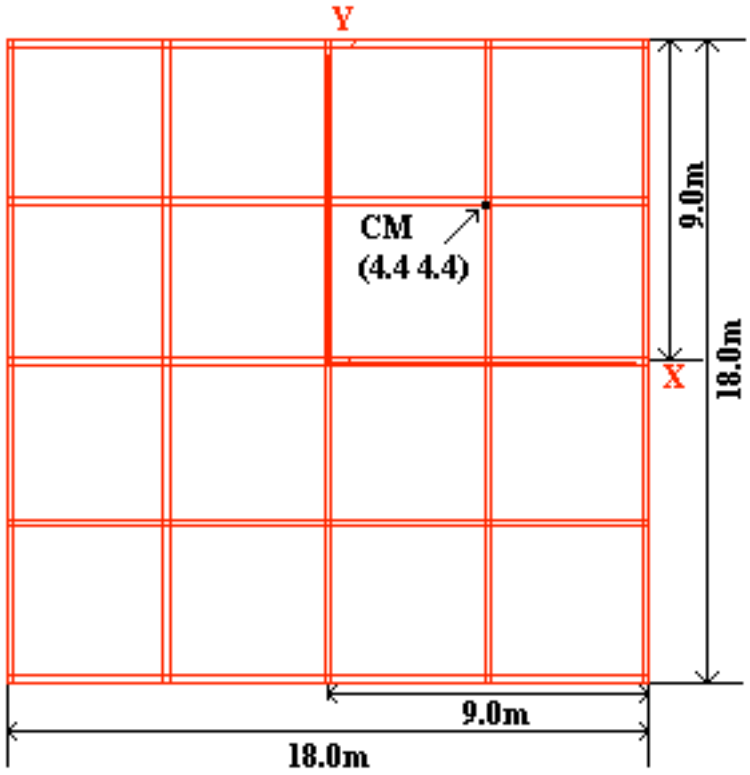

Fig. 7.3: The floor plan. The CM denotes the center of the mass, which located at (4.4 4.4) in the first quadrant, with O as the coordinate center.

7.2 Numerical results

In order to carry out the parametric study, a group of three buildings each with a one-level basement model, as shown in Figure 7.1, has been considered. The three buildings are of 5, 10 and 15 stories above ground. In this study, there are two types

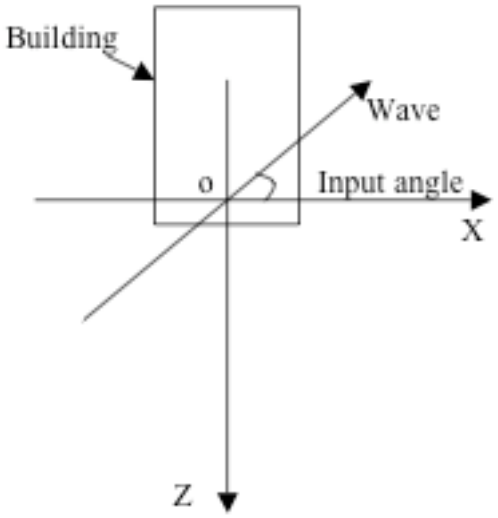

Fig. 7.4: The coordinate system. The input angle is defined as the angle between the wave propagation direction and X-axis. The building is mass asymmetrical.

of loading applied to the buildings. In the first part of the study, only the externally applied force will be applied bi-directionally to the center of the mass at the ground level. The harmonic and earthquake loadings are adopted from [41]. First, a sine wave is applied in the X-direction with the peak ground acceleration (PGA) equal to 0.80g and another sine wave is applied in the Y-direction with PGA equal to 0.50g, as shown in Figure 7.5. The loadings applied in X- and Y-direction are in phase. Second, in order to facilitate a comparison study with the harmonic loading case, the recordings of the 1940 El Centro earthquake are amplified by 2.29 times. Thus, amplified earthquake recordings with PGA equal to 0.80g in the NS component is applied in the X-direction and with PGA equal to 0.49g in the EW component is applied in the Y-direction, as shown in Figures 7.6-7.7. For both cases, the SSI effect is not taken into account. Here, we assume the earthquake recording station is close to the epicenter. The vertical component is not included in this comparison study. The NS and EW components of the recording data are assumed as the summary effect of earthquake waves including P, SH and SV waves. The contribution from each type of waves are not differentiated.

In the second part of the study, the amplified NS component of the 1940 El Centro earthquake recordings is used as the earthquake wave loading for studying the dynamic response of the two-way asymmetrical building with the inclusion of the soil-structure interaction effects. The loading point is chosen close to the origin of the coordinate system, where the earthquake loadings are applied. The input angle is measured from the positive X-axis in the direction of the wave propagation. The X-Z plane is the input plane for earthquake waves. The earthquake recordings are used directly as P, SH, and SV waves.

The response of buildings of different heights is compared and analyzed, including the soil-structure interaction. The relationships between the characteristics of the dynamic response of the buildings and the earthquake input are determined. The loading is on the ground level of the building to simulate the impacting of the adjacent soil. The incoming earthquake waves arrive from an arbitrary direction. The displacement of the building roof will be calculated and compared. The rotation of the building due to the mass eccentricity is also studied.

Furthermore, these results are compared with the cases of symmetrical buildings under the same loading conditions. The effect of the coupling between the asymmetrical building and bi-directional asymmetrical loadings is revealed through this comparison.

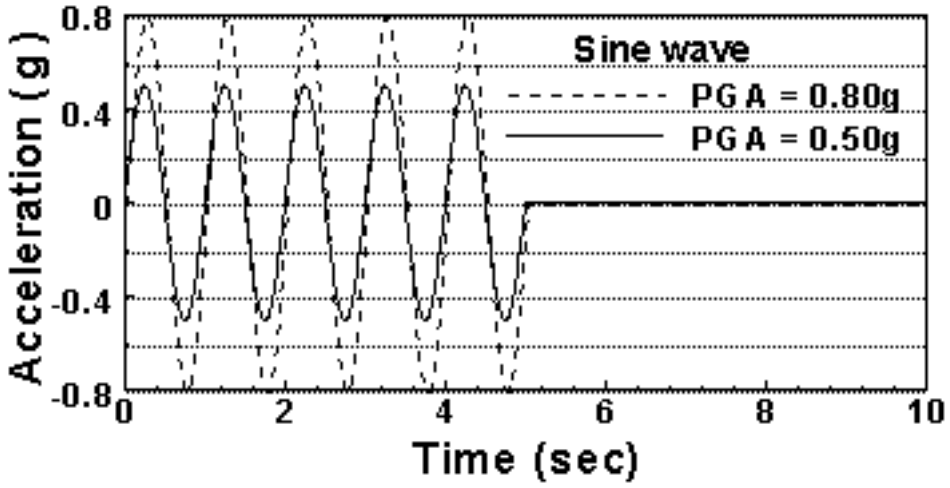

Fig. 7.5: The Sine waves with PGA equals to 0.80g and 0.50g.

7.2.1 Response to a harmonic loading and 1940 EI Centro earthquake loading

The response time histories of the building model subjected to the harmonic wave and earthquake loadings are obtained by using DSSIA-3D. Time histories of the center of the mass of the roof under the loading of sine wave with PGA=0.80g applied in the X-direction and PGA=0.50g applied in the Y-direction at the ground level. The variation of peak displacements in X, Y and Z-direction and rotation are shown in Figure 7.2.1 with the presence of earthquake loadings. The free vibration after the earthquake loading ceased is not given here. It is observed that the response of the asymmetrical building is close to a multiplication of harmonic waves, especially for a 5-story building. The response of the roof to the ground level loading is delayed by a few seconds.

Time histories of the center of the mass of the roof under the loading of El Centro earthquake with NS component applied in the X-direction and EW component applied in the Y-direction are shown in Figure 7.2.1. It can be seen that the response of the building is much more complex and random. In such a case, the damage to the structure would occur due to a large displacement in one direction. From both cases, we can conclude that the rocking in the X-Z plane dominates the building's response characteristics. By comparing the three buildings with different heights, the mass effect on the response of the buildings decreases with increasing height, especially

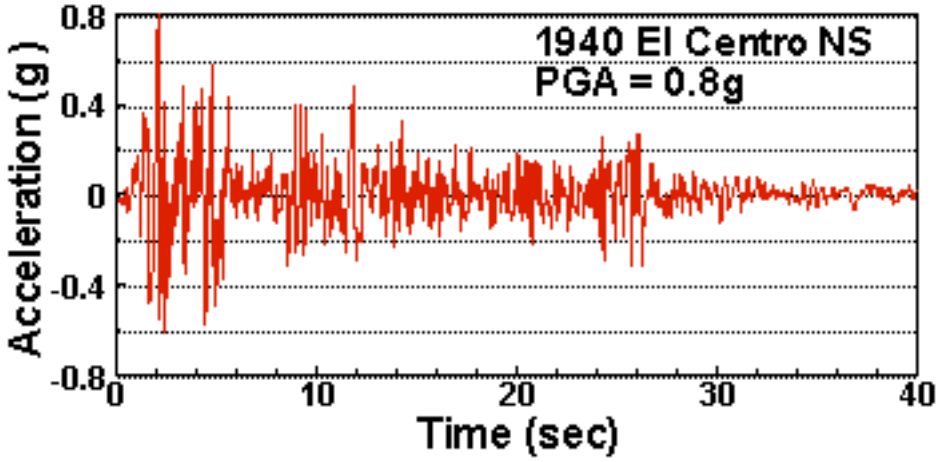

Fig. 7.6: 1940 El Centro Earthquake NS component applied in X direction.

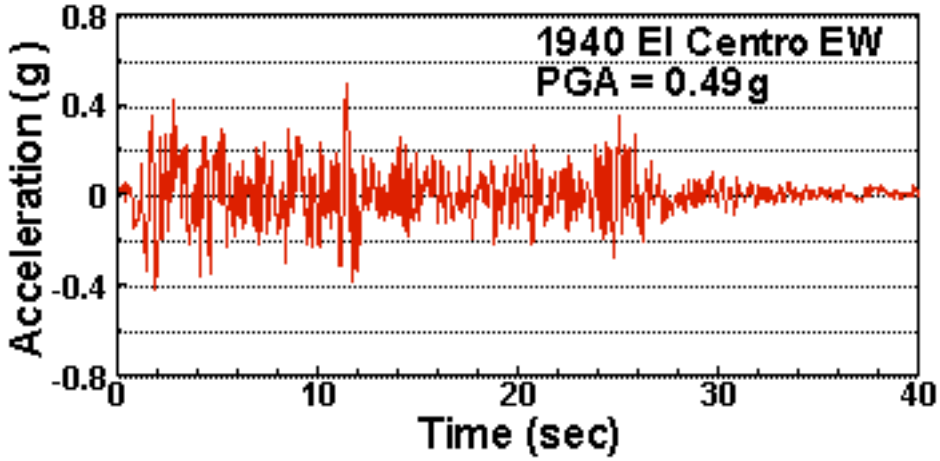

Fig. 7.7: 1940 El Centro Earthquake EW component applied in Y direction.

when the building is subjected to a non-harmonic loading.

7.2.2 Response to 1940 El Centro earthquake loading with SSI effect

In the second part of this study, the response of the same asymmetrical buildings subjected to an earthquake loading with SSI effect are obtained. We use the amplified NS component of the 1940 El Centro earthquake recordings as the earthquake loading and also assume it can be either one of the wave types, such as P, SH or SV wave. The frequency characteristic is the representative feature of this type of loading compared

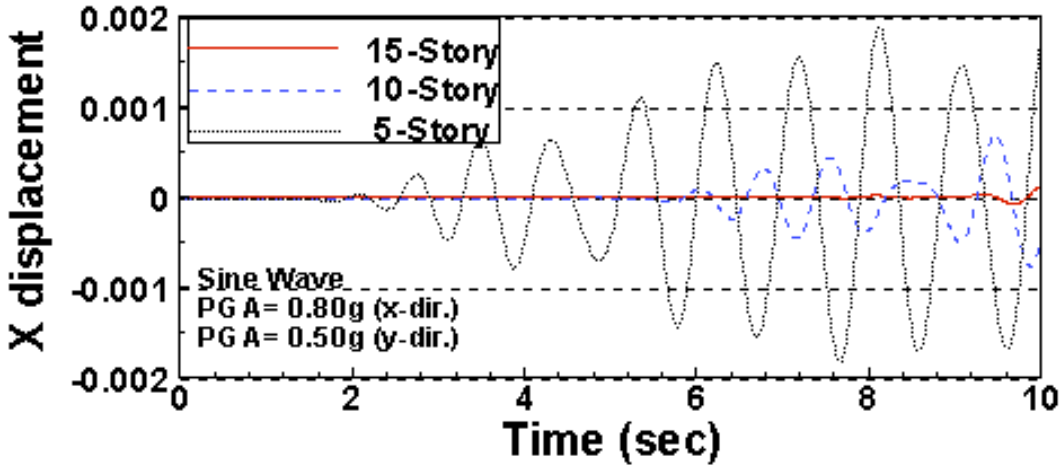

(A)

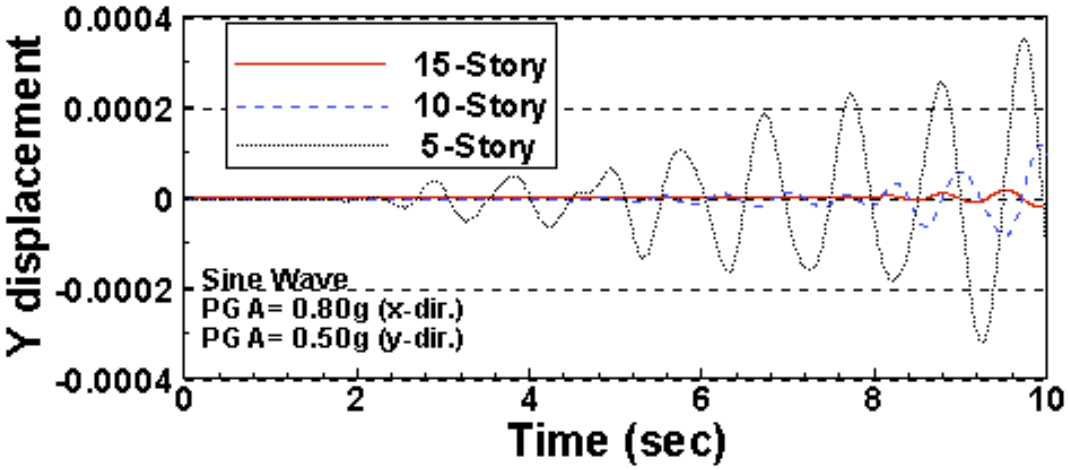

(B)

Figure 7.8: Time histories of the center of the mass of the roof under the loading of sine wave with PGA=0.80g applied in the X-direction and PGA=0.50g applied in the Y-direction at the ground level: (A) displacement in X direction; (B) displacement in Y direction; (C) displacement in Z direction; (D) rotation

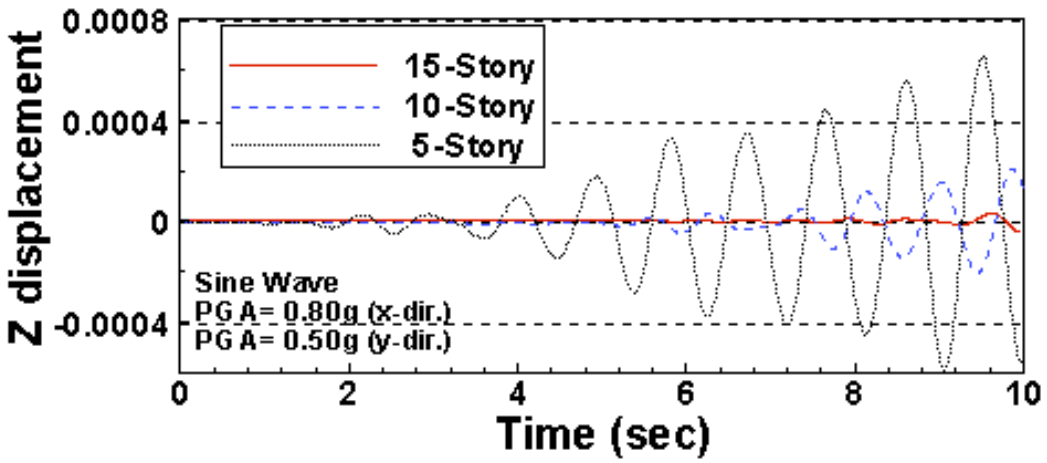
0.0008
0.0004
0
-0.0004
Z displacement
15-Story
10-Story
5-Story
Sine Wave
PGA= 0.80g (x-dir.)
PGA= 0.50g (y-dir.)
0
2
4
6
8
10
Time (sec)

(C)

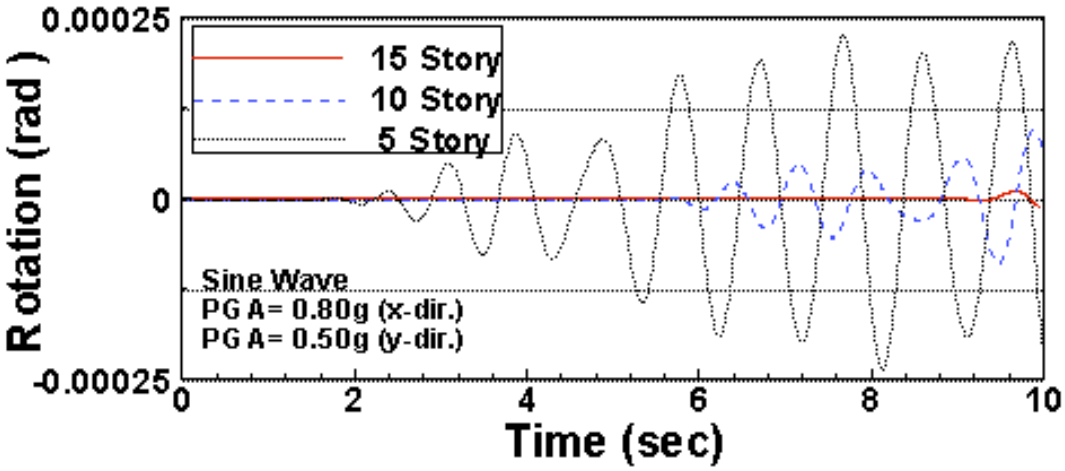
0.00025
0
-0.00025
Rotation (rad)
15 Story
10 Story
5 Story
Sine Wave
PGA= 0.80g (x-dir.)
PGA= 0.50g (y-dir.)
0
2
4
6
8
10
Time (sec)

(D)

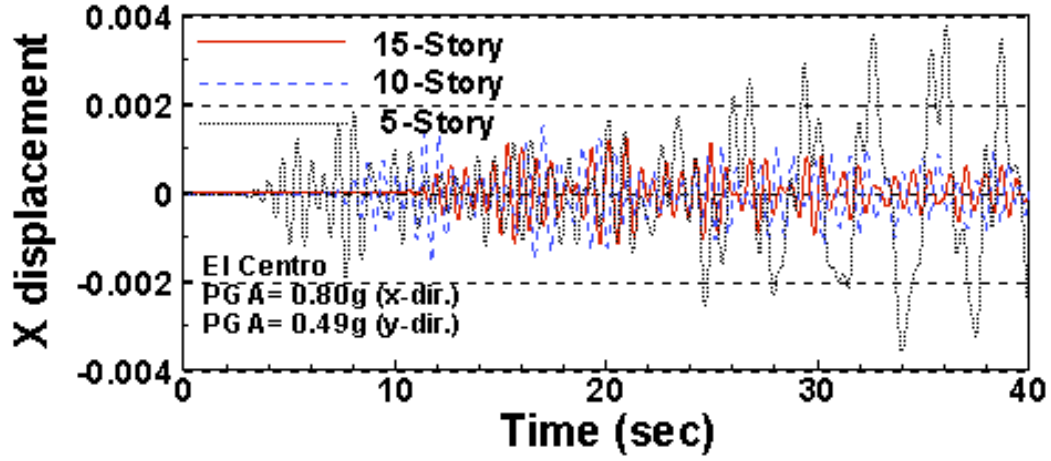

(A)

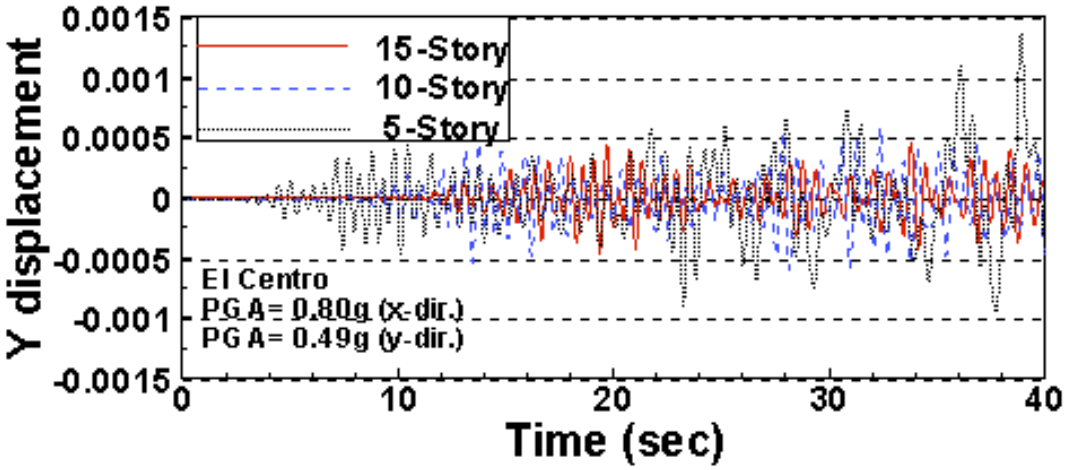

(B)

Figure 7.9: Time histories of the center of the mass of the roof under the loading of El Centro earthquake with NS component applied in the X-direction and EW component applied in the Y-direction: (A) displacement in X direction; (B) displacement in Y direction; (C) displacement in Z direction; (D) rotation

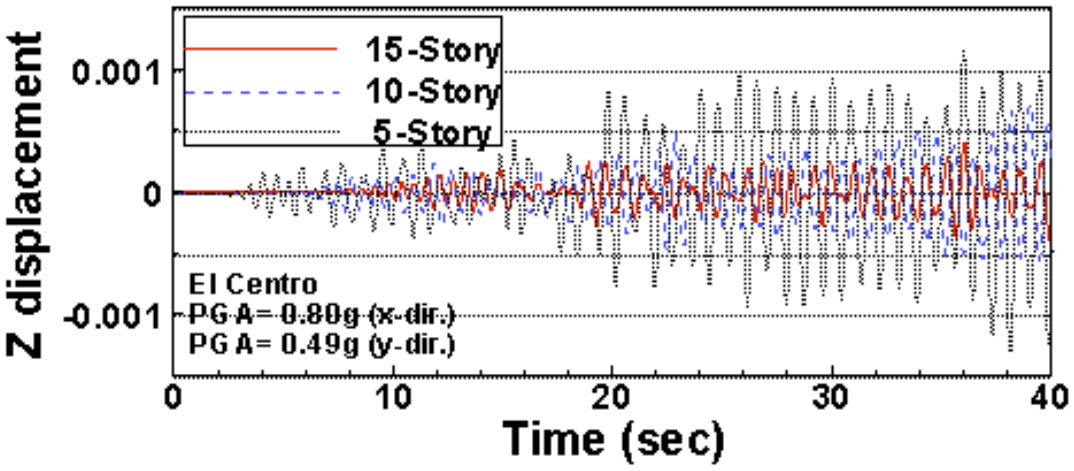
15-Story
10-Story
5-Story
El Centro
PGA= 0.80g (x-dir.)
PGA= 0.49g (y-dir.)
Z displacement
0.001
0
-0.001
0
10
20
30
40
Time (sec)

(C)

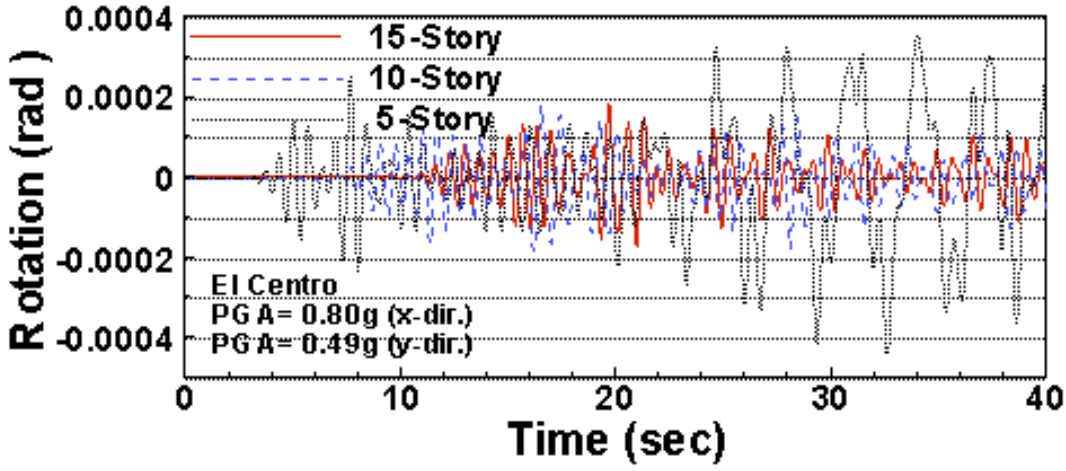
15-Story
10-Story
5-Story
El Centro
PGA= 0.80g (x-dir.)
PGA= 0.49g (y-dir.)
Rotation (rad)
0.0004
0.0002
0
-0.0002
-0.0004
0
10
20
30
40
Time (sec)

(D)

with a harmonic loading. Due to the similarity of the wave spectrum of P, SH and SV waves, we use only the N-S component of the earthquake recordings as the loading for P, SH and SV waves. The input angle for P waves varies from 30 to 90 degrees. The wave input plane is the XZ plane. Non-dimensional displacement of the center of mass of the asymmetrical building subjected to 1940 El Centro earthquake loadings in different wave types at different input angles are shown in Figure 7.2.2 for P waves with input angles of 30 degrees, 60 degrees and vertically, SH waves with an input angle of 60 degrees, SV waves with an input angle of 60 degrees. For P waves, it is observed that the displacement in the X direction decreases as the input angle increases. Because the ray path of P waves curves up, the building subjected to an input angle of 90 degrees is thus located further away from the epicenter compared with the building subjected to the impact of P waves with a smaller input angle. Here, we assume the only changing variable is the angle. Meanwhile, the dominant response shifts from X direction to vertical direction as the input angle increases.

For the same input angle of 60 degrees and to the same building, we can observe that the SV wave results in the same magnitude of displacement in the dominant X direction as for the P wave. This is explained by the concentration of kinetic energy of soil particles in the input X-Z plane for P waves and SV waves. However, for SH waves, the soil particles are vibrating in the perpendicular direction to the X-Z plane. The dominant displacement of the lower part of the building caused by the SV wave are about 5 times larger than that by the SH wave under the same conditions for the displacement in the X direction.

From the simulated results for both P waves and shear waves, at the lower level of the building, the large peak displacement is observed during the same period of the earthquake event. In such a short period time, the building is subjected to a strong ground motion. The building is under the condition of forced vibration. Large displacement and deformation of the lower level of the building are the consequence of the forced vibration. After a major earthquake, the collapse at the lower level of the building is often observed.

7.2.3 The building height factor

Subject to the same waves and angles of input, the response charactericstics of the different heights of buildings are compared, as shown in Figure 7.11. This study corresponds to the scenario where different height of buildings located in the same

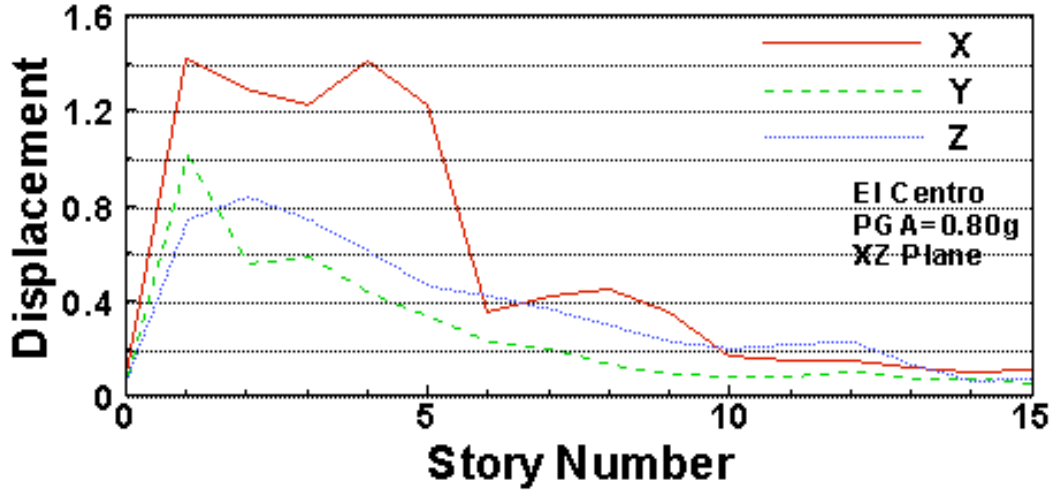

(A)

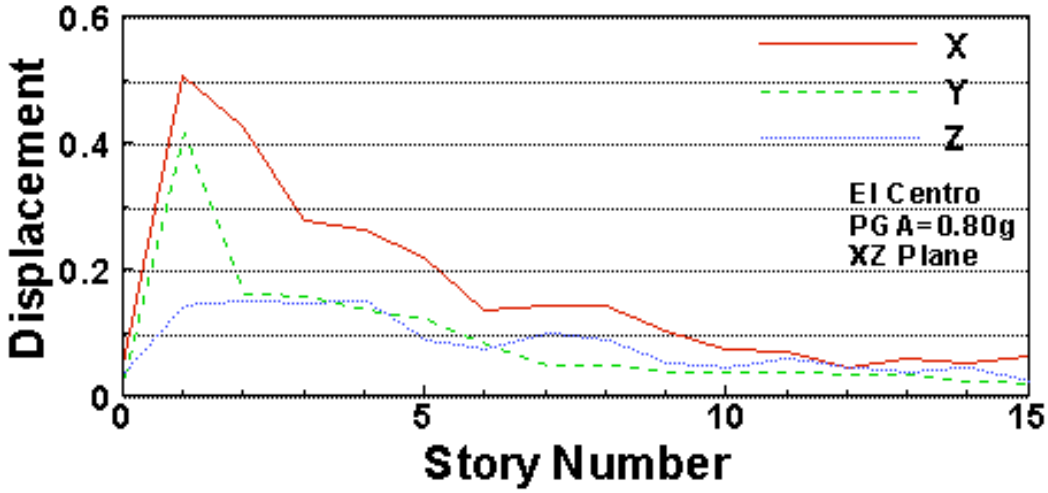

(B)

Figure 7.10: Non-dimensional displacement (x10^2) of the center of mass of the asymmetrical building subject to 1940 El Centro earthquake loadings in different wave types at different input angles: (A) P wave with input angle of 30^o; (B) P wave with input angle of 60^o; (C) P wave input vertically; (D) SH wave with input angle of 60^o; (E) SV wave with input angle of 60^o

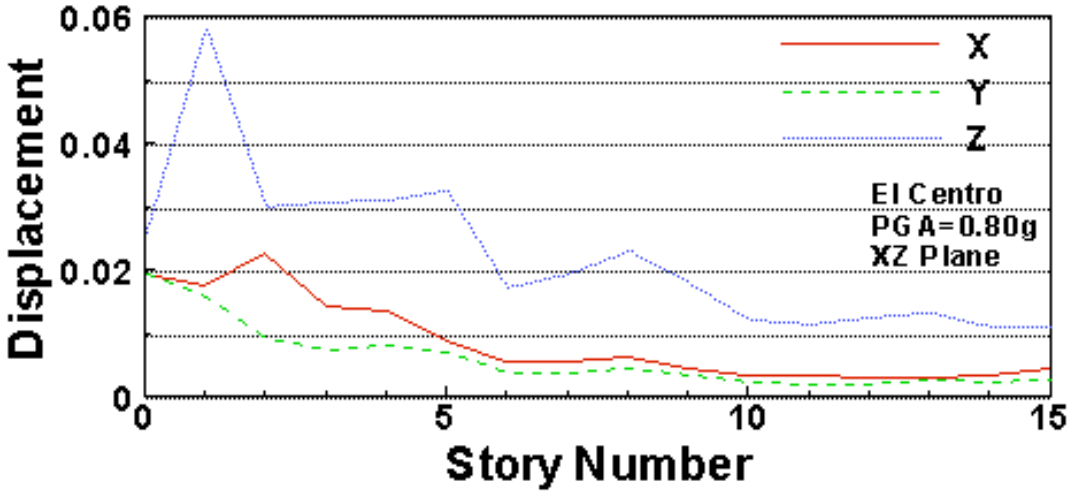
0.06
0.04
0.02
0
Displacement
0
5
10
15
Story Number
X
Y
Z
El Centro
PGA=0.80g
XZ Plane

(C)

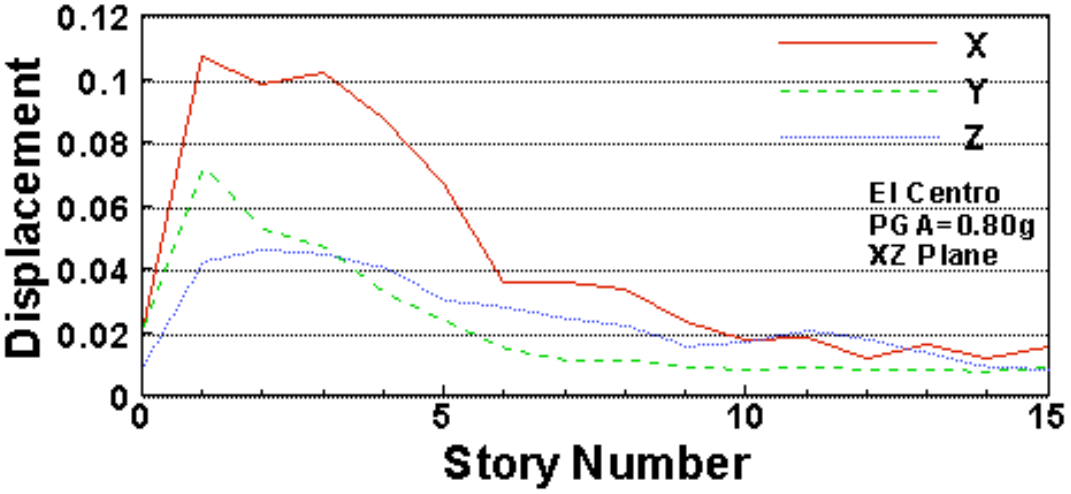
0.12
0.1
0.08
0.06
0.04
0.02
0
Displacement
0
5
10
15
Story Number
X
Y
Z
El Centro
PGA=0.80g
XZ Plane

(D)

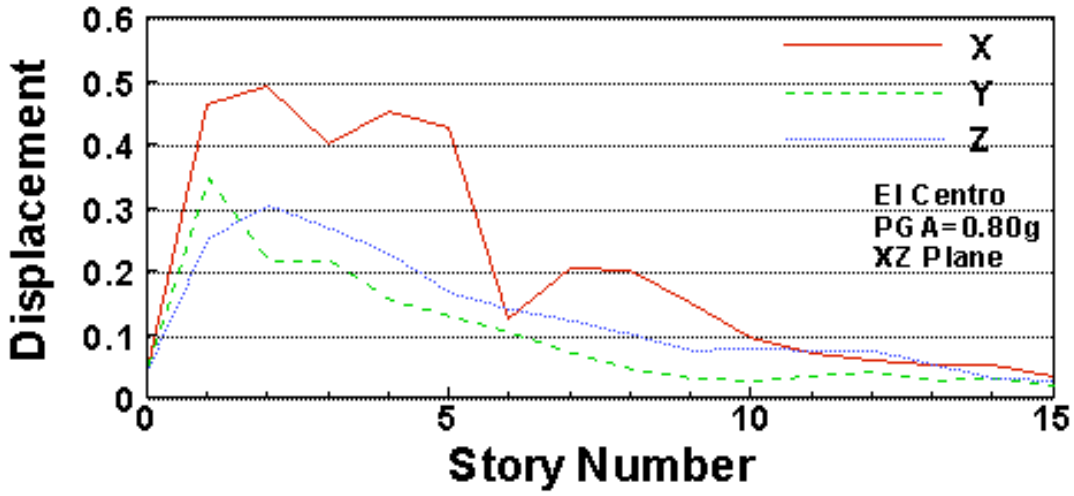

(E)

area during a major earthquake. With the only difference of building height as the variable, the different response to the same earthquake can be examined. Observed from the simulation, the dominant displacement is in the X-direction for P waves with input angles less than 60 degrees, or for the same strength of P waves at the further distance from the epicenter. The dominant displacement shifts to Z-direction, when P waves propagate vertically towards the building compared with the displacement in other directions. The largest displacement will result for cases of input P waves propagating close to surface. The same conclusion can be drawn for the shear wave cases. Especially for shorter buildings, such as the 5-level building, the peak displacement of the roof is larger than for other taller buildings. Also, the largest displacement usually can be found around the ground level. The low inertia of the low level building characterizes the large displacement of the whole building which is in contrast to the small displacement of the roof for taller buildings.

7.2.4 The comparison between asymmetrical and symmetrical buildings with SSI effect

In order to identify the significant influence from the mass eccentricity toward the building's response during earthquakes, the symmetrical building with even mass distribution is studied under the same bi-directional asymmetrical loading conditions. The mass eccentricity is the only influence examined here. A 15-story building is used

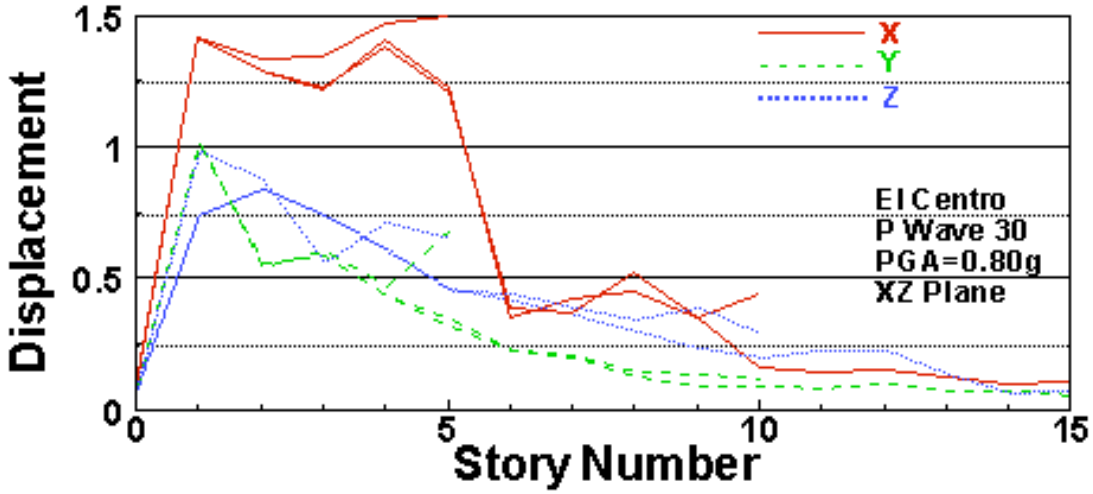
Displacement
1.5
1
0.5
0
0
5
10
15
Story Number
X
Y
Z
El Centro
P Wave 30
PGA=0.80g
XZ Plane

(A)

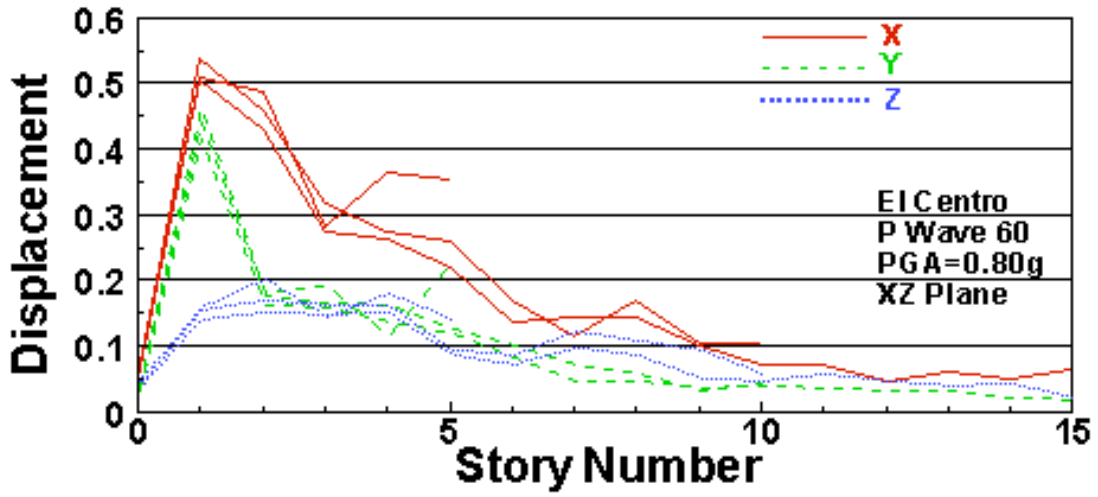
0.6
0.5
0.4
0.3
0.2
0.1
0
Displacement
0
5
10
15
Story Number
X
Y
Z
El Centro
P Wave 60
PGA=0.80g
XZ Plane

(B)

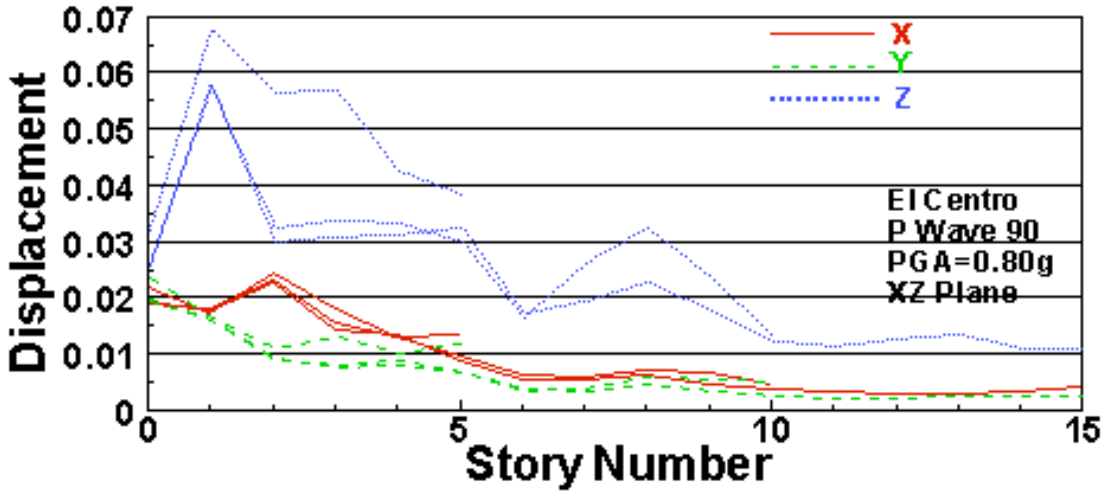
0.07
0.06
0.05
0.04
0.03
0.02
0.01
0
Displacement
0
5
10
15
Story Number
X
Y
Z
El Centro
P Wave 90
PGA=0.80g
XZ Plane

(C)

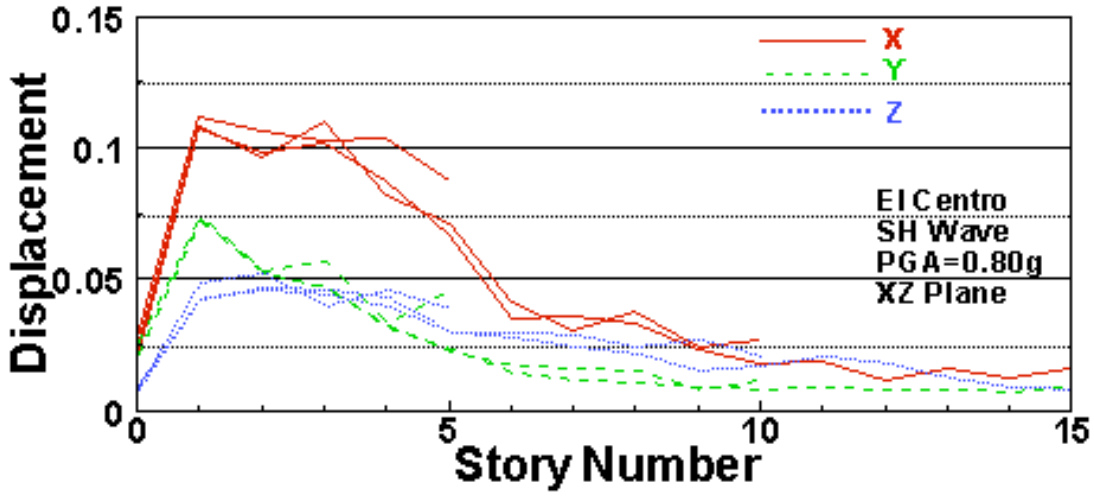

(D)

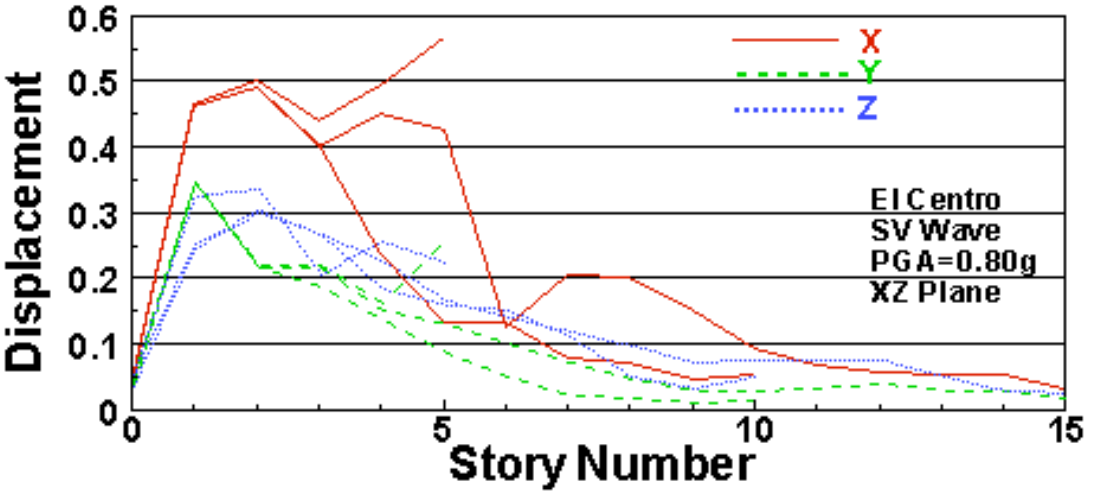

(E)

Fig. 7.11: Non-dimensional displacement (x10^2) of the center of mass of the asymmetrical building with different height subject to 1940 El Centro earthquake loadings: (A) P wave at an input angle of 30^o; (B) P wave at an input angle of 60^o; (C) P wave at an input angle of 90^o; (D) SH wave at an input angle of 60^o; (E) SV wave at an input angle of 60^o.

for this purpose without loss of the generalization.

For comparison, both nodal points in the symmetrical building and asymmetrical building are chosen with the same coordinates. Under the same loading conditions, the asymmetrical building has larger displacements than the symmetrical building overall, especially in the X and Z direction. The uneven mass distribution is the only factor that contributes to the larger displacement in the asymmetrical building. For different types of waves, the P and SV waves result in a much stronger response from the building than the SH waves do, as shown in Figure 7.12. The displacement in the X and Y direction caused by P and SV waves is about 5 times larger than those caused by SH waves. This is consistent with the observation made earlier from the symmetrical building cases. Hayashi et al [23] studied three buildings damaged in the 1995 Kobe, Japan, earthquake and observed the tall building with an asymmetrical-plan configuration of the core suffered more damages than the corresponding symmetrical-plan case. The noticeable shear cracks of the reinforced concrete walls appear from 4th to 6th floor of the building with 13 stories and from 2nd to 7th floor of another building with 11 stories. These observations verify the conclusion that the lower floors suffer most damages. Furthermore, the direction of the damages is perpendicular to the dilatational wave propagation direction. Again, these verify the findings from the dynamic wave-soil-structure interaction analysis of both symmetrical and asymmetrical tall buildings that shear waves cause more damages to structures than the primary waves.

7.3 Conclusion for two-way asymmetrical building

The dominant earthquake wave components coupled with the eccentric character of the building determines the response characteristics of the buildings. The lower to medium sized buildings incurred the most impact from the earthquakes. The mass effect is not a major factor for tall buildings. The asymmetrical building coupled with the two-way asymmetrical earthquake loadings will amplify the damages to the structure compared with symmetrical buildings. These results are consistent with field observations after major earthquakes. This explains the vulnerability of asymmetrical buildings during earthquakes. Seismic resistance measures, such as supplemental viscous damping or energy dissipation devices, as recommended by [18]. Further experiments on soil dynamic properties and building vibration elements will help to increase the accuracy of the numerical model. Also, improvement in computing

hardware and numerical algorithms will increase both the accuracy and confidence of the results. The contact problem of the soil and structure is another direction for a detailed understanding of the mechanism of the soil-structure interaction, such as yielding of the support soil, development of gaps, and slipping and uplifting of the foundation. This study is helpful for designing new earthquake resistant structures to reduce damage.

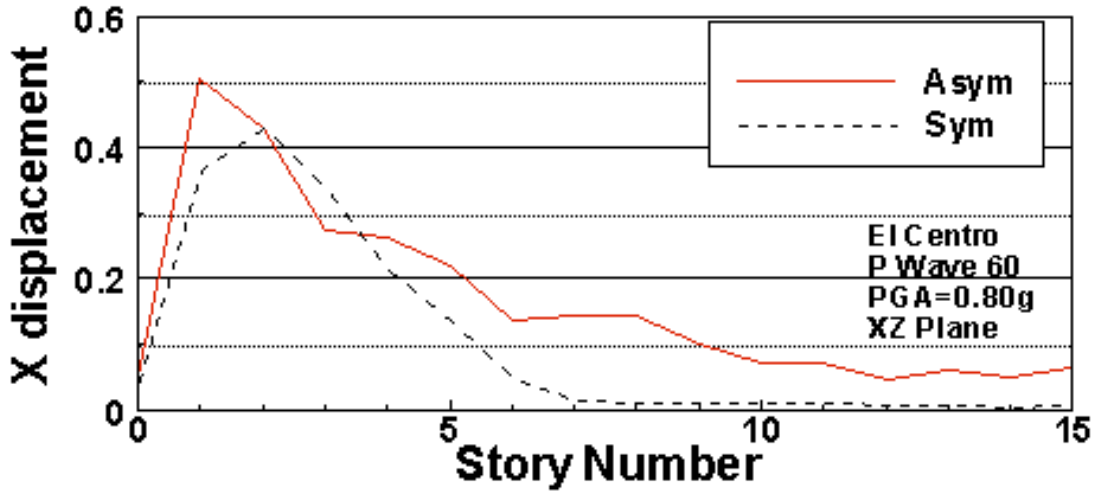
X displacement
0.6
0.4
0.2
0
0
5
10
15
Story Number
Asym
Sym
El Centro
P Wave 60
PGA=0.80g
XZ Plane

(A)

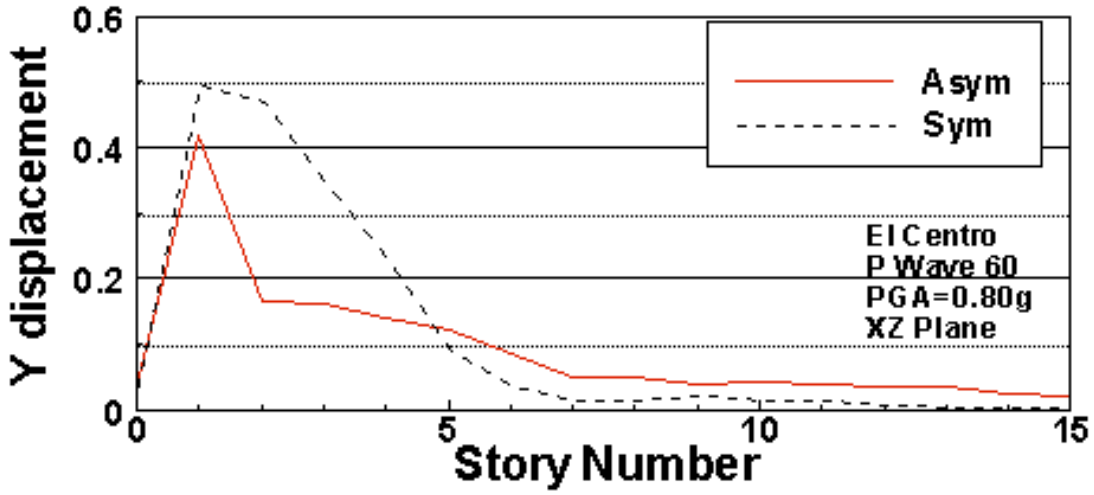
Y displacement
0.6
0.4
0.2
0
0
5
10
15
Story Number
Asym
Sym
El Centro
P Wave 60
PGA=0.80g
XZ Plane

(B)

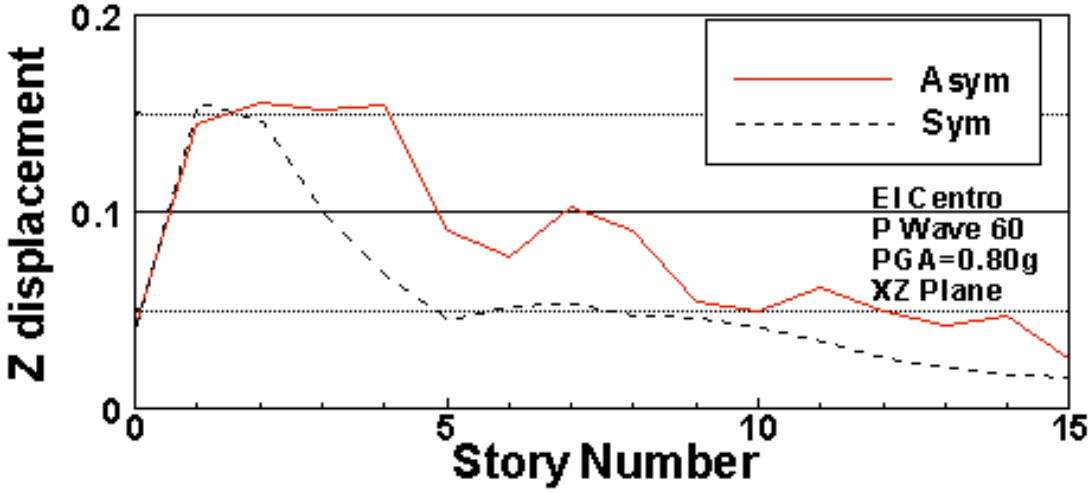
0.2
0.1
0
Z displacement
0
5
10
15
Story Number
Asym
Sym
El Centro
P Wave 60
PGA=0.80g
XZ Plane

(C)

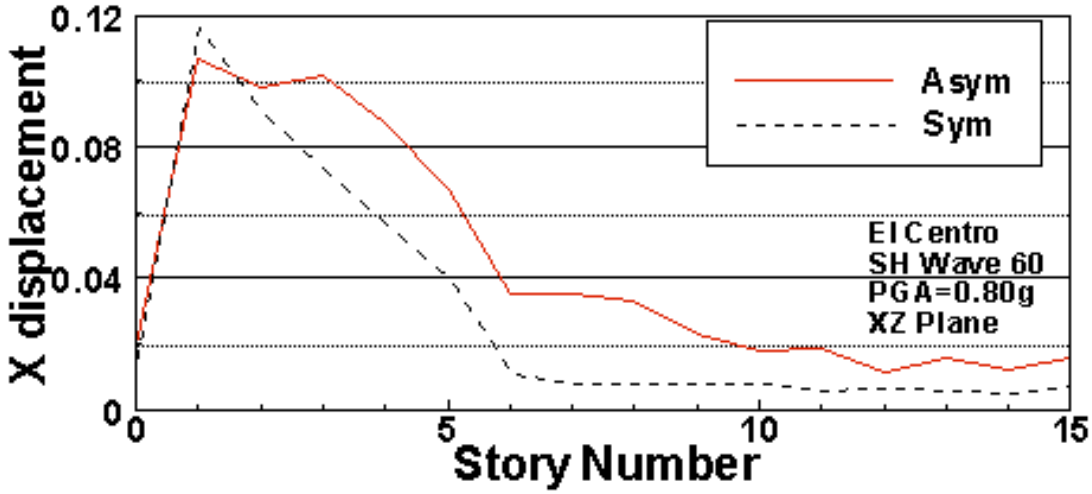
0.12
0.08
0.04
0
X displacement
0
5
10
15
Story Number
Asym
Sym
El Centro
SH Wave 60
PGA=0.80g
XZ Plane

(D)

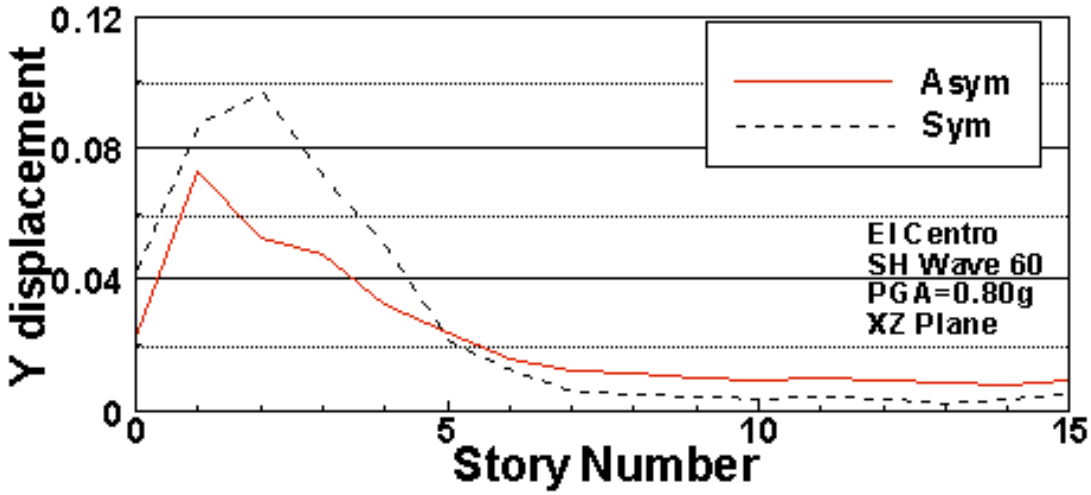
0.12
0.08
0.04
0
Y displacement
0
5
10
15
Story Number
Asym
Sym
El Centro
SH Wave 60
PGA=0.80g
XZ Plane

(E)

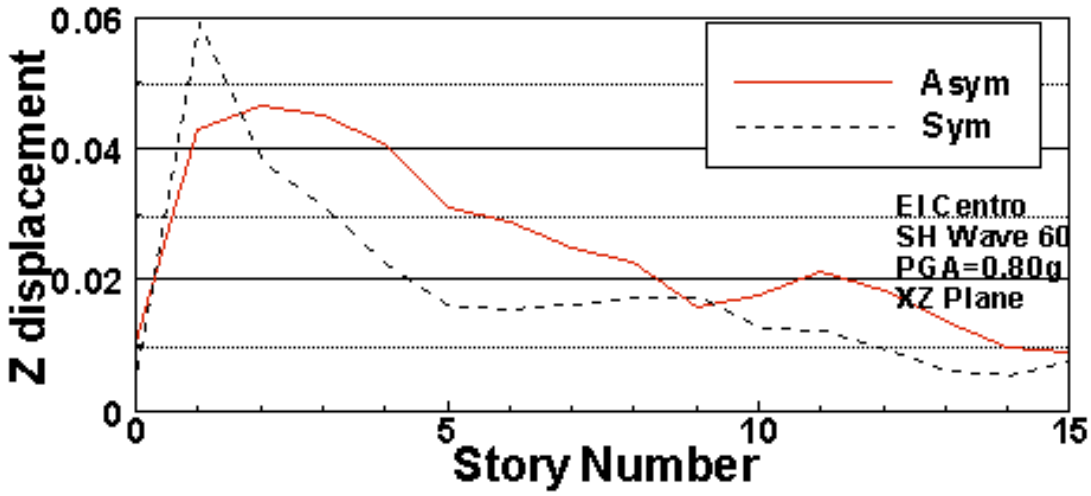
0.06
0.04
0.02
0
Z displacement
0
5
10
15
Story Number
Asym
Sym
El Centro
SH Wave 60
PGA=0.80g
XZ Plane

(F)

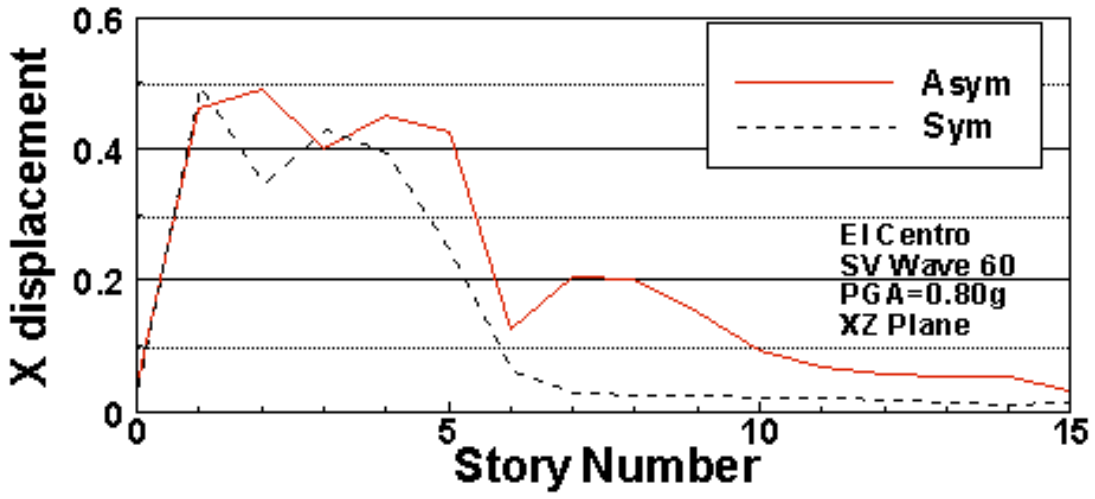
X displacement
0.6
0.4
0.2
0
0
5
10
15
Story Number
Asym
Sym
El Centro
SV Wave 60
PGA=0.80g
XZ Plane

(G)

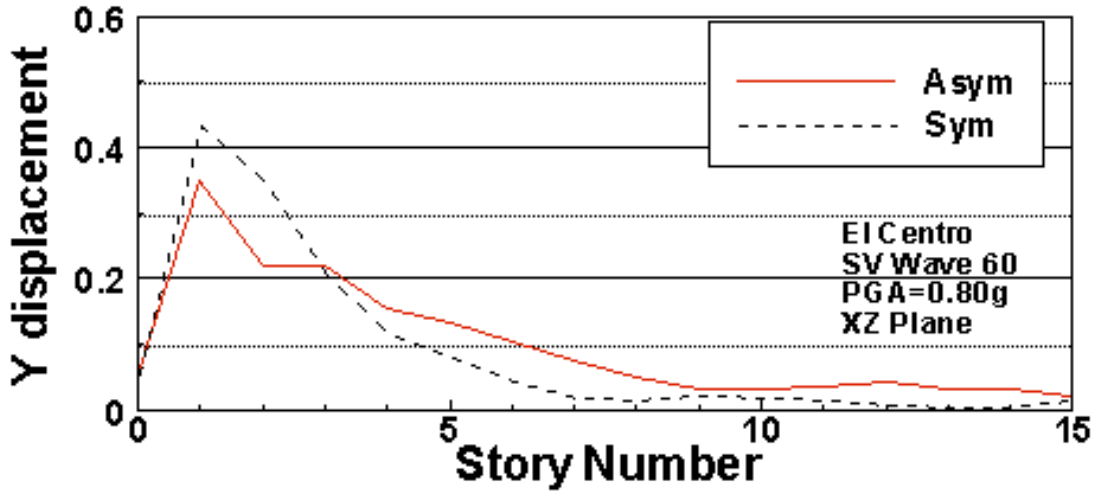
Y displacement
0.6
0.4
0.2
0
0
5
10
15
Story Number
Asym
Sym
El Centro
SV Wave 60
PGA=0.80g
XZ Plane

(H)

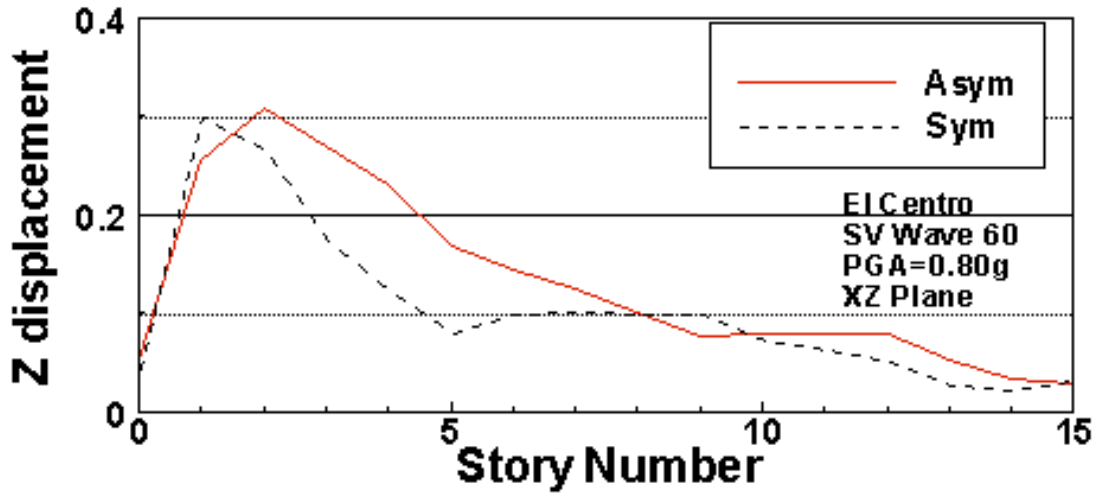

(I)

Fig. 7.12: Non-dimensional displacement (x10^2) of the center of mass of the 15-story symmetrical building subject to 1940 El Centro earthquake loadings: (A) P wave with input angle of 60^o in the X direction; (B) P wave with input angle of 60^o in the Y direction; (C) P wave with input angle of 60^o in the Z direction; (D) SH wave with input angle of 60^o in the X direction; (E) SH wave with input angle of 60^o in the Y direction; (F) SH wave with input angle of 60^o in the Z direction; (G) SV wave with input angle of 60^o in the X direction; (H) SV wave with input angle of 60^o in the Y direction; (I) SV wave with input angle of 60^o in the Z direction.

Chapter 8

Conclusion on Contributions

The vibration of tall buildings with symmetrical or asymmetrical configuration is simulated for both harmonic loadings and real earthquake loadings. Both are published in a series of conferences and journal papers. The influence from different soil types to the earthquake response of tall buildings is investigated. The fundamental frequencies and equivalent damping ratios are calculated and studied for revealing the soil-structure interaction effect. In general, the mass asymmetrical tall buildings suffers more damages than the corresponding symmetrical buildings. This indicates the symmetrical building is more seismic resistant than an asymmetrical building in an earthquake.

Bibliography

[1] Aki K. and Richards P. G. *Quantitative seismology: theory and methods* W. H. Freeman and Company, San Francisco, California, 1980.

[2] Alyagshi Eilouch M. N. and Sandhu R. S. A mixed method for transient analysis of soil-structure interaction under SH-motion *Earthquake Engineering and Structural Dynamics* Vol. 14, pp. 499-516, 1986.

[3] Armando B. and Luis E. Influence of dynamic soil-structure interaction on the nonlinear response and seismic reliability of multistorey systems *Earthquake Engineering and Structural Dynamics* Vol. 36, pp. 327-346, 2007.

[4] Arnold D., Kerr S.E. and Magdy A. Validation of new equations for dynamic analysis of tall frame-type structures *Earthquake Engineering and Structural Dynamics* Vol. 15, pp. 549-563, 1987.

[5] Bathe Klaus-Jurgen, *Finite element procedures* Prentice-Hall, Inc. Englewood Cliffs, New Jersey, 1996.

[6] Belytschko T., Krongauz Y., Organ D. et al. Meshless methods: an overview and recent developments *Computational Methods in Applied Mechanical Engineering* Vol. 139, pp. 1-47, 1996.

[7] Benedetti D., Carydis P. and Pezzoli P. Shaking table tests on 24 simple masonry buildings *Earthquake Engineering and Structural Dynamics* Vol. 27, pp. 67-70, 1998.

[8] Brownjohn M. W., Pan T. C. and Deng X. Y. Correlating dynamic characteristics form field measurements and numerical analysis of a high-rise building *Earthquake Engineering and Structural Dynamics* Vol. 29, pp. 523-543, 2000.

[9] Bryan S.S. and Elizabeth C. Estimating periods of vibration of tall buildings *Journal of Structural Engineering* Vol. 112, pp. 1005-1019, 1986.

[10] Capuani D., Klein R., Antes H. and Tralli A. Dynamic soil-structure interaction of coupled shear walls by boundary element method *Earthquake Engineering and Structural Dynamics* Vol. 24, pp. 861-879, 1995.

[11] Chajes M.J., Zhang L. and Kirby J.T. Dynamic analysis of tall build-ing using reduced-order continuum model *Journal of Structural Engineering* Vol. 122, pp. 1284-1291, 1996.

[12] Chandler A. M. and Duna X. N. Evaluation of factors influencing the inelastic seismic performance of torsionally asymmetric building *Earthquake Engineering and Structural Dynamics* Vol. 20, pp. 87-95, 1991.

[13] Chapel F. Boundary element method applied to linear soil-structure interaction on a heterogeneous soil *Earthquake Engineering and Structural Dynamics* Vol. 15, pp. 815-829, 1987.

[14] Chen J. *Analysis of local variations in free field seismic ground motion* Ph.D. Dissertation, 1980, University of California, Berkeley.

[15] Eshraghi H. and Dravinski M. Scattering of plane harmonic SH, SV, P and Rayleigh waves by non-axisymmetric three-dimensional canyons: a wave function expansion ap-proach *Earthquake Engineering and Structural Dynamics* Vol. 18, pp. 983-998, 1989.

[16] Fluge W. *Viscoelasticity* Blasisdell Publishing Company 1967, USA.

[17] Fukui T. Time marching BE-FE method in 2-D elastodynamic problem International conference on BEM IX Stuttgart, 1987.

[18] Goel R.K. Effects of supplemental viscous damping seismic response of asymmetric-plan systems *Earthquake Engineering and Structural Dynamics* Vol. 27, pp. 125-141, 1998.

[19] Goldberg J.E., Bogdanoff J.L. and Lee M.Z. Forced vibration and natu-ral frequencies of tall building frames *Bulletin of the Seismological Society of America* Vol. 49, pp. 33-47, 1959.

[20] Hao H., Ma G.W. and Lu Y. Damage assessment of masonry infilled RC frames subjected to blasting induced ground excitations *Engineering Structures* Vol. 24, pp. 799-809, 2002.

[21] Hart, Gary C. and Wong K. *Structural Dynamics for Structural Engineers* John Wiley & Sons, 1999.

[22] Hassan A. and Dakoulas P. Non-linear dynamic earth dam-foundation interaction using BE-FE method *Earthquake Engineering and Structural Dynamics* Vol. 27, pp. 917-936, 1998.

[23] Hayashi Y., Tamura K., Mori M. and Takahashi I. Simulation analysis of buildings damaged in the 1995 Kobe, Japan, Earthquake considering soil-structure interaction *Earthquake Engineering and Structural Dynamics* Vol. 28, pp. 371-391, 1999.

[24] Hejal R. and Chopra A. K. Earthquake analysis of a class of torsionally coupled buildings *Earthquake Engineering and Structural Dynamics* Vol. 18, pp. 305-323, 1989.

[25] Housener G.W. and Brady A. G. Natural periods of vibration of buildings *Journal of Engineering Mechanics Division Proceedings of the American Society of Civil Engineers* August, pp. 31-65, 1963.

[26] Israil A. S. M. and Banerjee P. K. Effects of geometrical and material properties on the vertical vibration of 3-D foundations by BEM *International Journal Numerical Analysis Methods in Geomechanics* Vol. 14, pp. 49-70, 1990.

[27] Jacobsen Lydik S. Natural periods of uniform cantilever beams *American Society of Civil Engineers Transactions* (Paper No. 2025) pp. 402-431, 1933.

[28] Jennings P.C. and Skattum K. S. Dynamic properties of planar coupled shear walls *Earthquake Engineering and Structural Dynamics* Vol. 1, pp. 387-405, 1973.

[29] Kan C. L. and Chopra A. K. Elastic earthquake analysis of torsionally coupled multi-story buildings *Earthquake Engineering and Structural Dynamics* Vol. 5, pp. 395-412, 1977.

[30] Kan C. L. and Chopra A. K. Simple model for earthquake response studies of torsionally coupled buildings *Journal of Engineering Mechanics Division ASCE* Vol. 107, pp. 935-951, 1981.

[31] Kiyoshi K. and Shizuyo Y. On the period and the damping of vibration of actual buildings *Bulletin of the Earthquake Research Institute* Vol. 39, pp. 477-489, 1961.

[32] Kanok-Nukulchai W.L., Sek Y. and Karasudhi P. A versatile finite strip model for three-dimensional tall building analysis *Earthquake Engineering and Structural Dynamics* Vol. 11, pp. 149-166, 1983.

[33] Karabalis D. L. and Beskos D. E. Dynamic response of 3-D flexible foundations by time domain BEM and FEM *Soil Dynamics and Earthquake Engineering* Vol. 4, pp. 91-101, 1985

[34] Kausel E. Local transmitting boundaries *Journal of Engineering Mechanics ASCE* 114, pp. 1011-1027, 1988.

[35] Kausel E., Rosset J. M. and Wass G. Dynamic analysis of footings on layered media *Journal of Engineering Mechanics ASCE* Vol. 101, pp. 679-693, 1975.

[36] Kawakami H. Rocking compliance functions for rigid bases allowed to uplift *Journal of Geotechnical Engineering* Vol. 116, pp. 725-739, 1990.

[37] Lambros S. and Katafygiotis C.P. Dynamic response variability of structures with uncertain properties *Earthquake Engineering and Structural Dynamics* Vol. 25, pp. 775-793, 1996.

[38] Li Q.S., Fang J.Q., Jeary A.P., Wong C.K. and Liu D.K. Evaluation of wind effects on a supertall building based on full-scale measurements *Earthquake Engineering and Structural Dynamics* Vol. 29, pp. 1845-1862, 2000.

[39] Hao H., Ma G.W. and Lu Y. A transmitting boundary for the numerical simulation of elastic wave propagation problems *Journal of Computational Physics* Vol. 3, pp. 174-183, 1984.

[40] Liu G.R. *Mesh free methods: moving beyond the finite element method* CRC Press, 2003.

[41] Lin J. L. and Tsai K.C. Seismic analysis of two-way asymmetric building systems under bi-directional seismic ground motions *Earthquake Engineering and Structural Dynamics* Vol. 37, pp. 305-328, 2008.

[42] Luco J.E. Soil-structure interaction and identification of structural models *Proceedings of the 2nd ASCE Conference on Civil Engineering and Nuclear Power* Vol 2, pp. 10/1/1-10/1/31, 1980.

[43] Lysmer J. and Kuhlemeyer R.L. Finite dynamic model for infinite media *Journal of Engineering Mechanics Division ASCE* Vol. 95, pp. 859-877, 1969.

[44] MeCallen D.B. and Romastad K. M. Nonlinear model for building-soil systems *Journal of Engineering Mechanics ASCE* Vol. 120 No. 5, pp. 1129-1152, 1992.

[45] Mossessian T.K. and Dravinski M. Application of a hybrid method for scattering of P, SV, and Rayleigh waves by near-surface irregularities *Bulletin of the Seismological Society of America* Vol. 77, pp. 1784-1803, 1987.

[46] Myslimaj B. and Tso W. W. A strength distribution criterion for minimizing torsional response of asymmetric wall-type systems *Earthquake Engineering and Structural Dynamics* Vol. 31, pp. 99-120, 2002.

[47] Nagashima I.M.R., Asami Y., Hirai J. and Abiru H. Performance of hybrid mass damper system applied to a 36-story high-rise building *Earthquake Engineering and Structural Dynamics* Vol. 30, No. 11, pp. 1615-1637, 2001.

[48] Nakamura Y., Tanaka K., Nakayama M. and Fujita T. Hybrid mass dampers using two types of electric servomotors: AC servomotors and linear-induction servomotors *Earthquake Engineering and Structural Dynamics* Vol. 30, No. 11, pp. 1719-1743, 2001.

[49] Prevost J.H. and Popescu R. Constitutive relations for soil materials *The Electronic Journal of Geotechnical Engineering* Vol. 1, 1996. Website: http://www.ejge.com

[50] Psycharis I. N. and Jennings P.C. Rocking of slender rigid bodies allowed to uplift *Earthquake Engineering and Structural Dynamics* Vol. 11, pp. 57-76, 1983.

[51] Rodriguez M.E. and Montes R. Seismic response and damage analysis of buildings supported of flexible soils *Earthquake Engineering and Structural Dynamics* Vol. 29, pp. 647-665, 2000.

[52] Rucker W. Dynamic behaviour of rigid foundations of arbitrary shape on a half-space *Earthquake Engineering and Structural Dynamics* Vol. 10, pp. 675-690, 1982.

[53] Safak E. Detection and identification of soil-structure interaction in buildings from vibration recordings *Journal of Structural Engineering* Vol. 121, pp. 899-906, 1995.

[54] Saito T., Shiba K. and Tamura K. Vibration control characteristics of a hybrid mass damper system installed in tall buildings *Earthquake Engineering and Structural Dynamics* Vol. 30, pp. 1677-1696, 2001.

[55] Sanchez-Sesma and Francisco J. Diffraction of elastic waves by three-dimensional sur-face irregularities *Bulletin of the Seismological Society of America* Vol. 73, No. 6, pp. 1621-1636, 1983.

[56] Sarma S. K. and Srbulov M. A simplified method for prediction of kinematic soil-foundation interaction effects on peak horizontal acceleration of a rigid foundation *Earthquake Engineering and Structural Dynamics* Vol. 25, No. 8, pp. 815-836, 1996.

[57] Shah A.H., Wong K.C., and Datta S.K. Diffraction of plane SH waves in a half-space *Earthquake Engineering and Structural Dynamics* Vol. 10, pp. 519-528, 1982.

[58] Shakib H. and Datta T. K. Inelastic response of torsionally coupled system to an ensemble of non-stationary ground motion *Engineering Structures* Vol. 15, pp. 13-20, 1993.

[59] Shakib H. and Fuladgar A. Dynamic soil-structure interaction effects on the seismic response of asymmetric buildings *Soil Dynamics and Earthquake Engineering* Vol. 24, pp. 379-388, 2004.

[60] Shakib H. and Touhidi R. Z. Evaluation of accidental eccentricity in buildings due to rotational components of earthquake *Earthquake Engineering* Vol. 6, pp. 431-445, 2002.

[61] Smith W.D. A nonreflecting plane boundary for wave propagation problems *Journal of Computational Physics* Vol. 15, pp. 492-503, 1974.

[62] Song C. and Wolf J. P. Consistent infinitesimal finite-element cell method: three-dimensional vector wave equation *International Journal for Numerical Methods in Engineering* Vol. 39, pp. 2189-2208, 1996.

[63] Song C. and Wolf J.P. The scaled boundary finite-element method-alias consistent infinitesimal finite-element cell method for elastodynamics *Computer Methods in Applied Mechanics and Engineering* Vol. 147, pp. 329-355, 1997.

[64] Spyrakos C. C. and Beskos D. E. Dynamic response of flexible strip foundations by boundary and finite elements *Soil Dynamics and Earthquake Engineering* Vol. 5, pp. 84-96, 1986.

[65] Stewart J.P. and Fenves G.L. System identification for evaluating soil-structure interaction effects in buildings from strong motion recordings *Earthquake Engineering and Structural Dynamics* Vol. 27, pp. 869-885, 1998.

[66] Takemori T., Sotomura K. and Yamada M. Nonlinear dynamic response of reactor containment *Nuclear Engineering and Design* Vol. 38, pp. 463-474, 1976.

[67] Takeuchi H. and Saito M. *Seismic surface waves* Methods in Computational Physics Vol. 11, B. A. Bolt, Editor, Academic Press, New York. 1972.

[68] Tehranizadeh M. Soil-structure interaction of tall building *Proceedings 11th European Conference on Earthquake Engineering* Paris 1998; Rotterdam: Balkema.

[69] Toki K. and Fu C. S. Generalized method for non-linear seismic response analysis of a three dimensional soil-structure interaction system *Earthquake Engineering and Structural Dynamics* Vol. 15, pp. 945-961, 1987.

[70] Uang C., Bertero V.V. and Clough R.W. Correlation studies using the equivalent base horizontal acceleration method *Earthquake Engineering and Structural Dynamics* Vol. 18, pp. 33-47, 1989.

[71] Uniform Building Code In: Int. Conf. Build. Off. Whitter, California, 1997.

[72] Von Estorff O. and Kausel E. Coupling of boundary and finite elements for soil-structure interaction problems *Earthquake Engineering and Structural Dynamics* Vol. 18, No. 7, pp. 1065-1075, 1989.

[73] Von Estorff O. and Prabucki M.J. The coupling of boundary and finite elements to solve transient problems in elastodynamics *Boundary Elements X* Vol. 4. pp. 447-450, Edited by Brebbia, C. A., Heidelberg, New York, Springer Verlag, 1988.

[74] Wass G. *Linear two-dimensional analysis of soil dynamics problems in semi-infinete layered media* Ph.D. thesis, University of California, Berkeley, California, 1972.

[75] Wegner J.L. Propagation of waves from a spherical cavity in an unbounded linear viscoelastic solid *International Journal of Engineering Science* Vol.31, No. 3, pp. 493-508, 1993.

[76] Wegner J.L. and Haddow J.B. A note on plane wave propagation in a linear viscoelastic solid *International Journal of Engineering Science* Vol. 27, No. 12, pp. 1545-1551, 1989.

[77] Wegner J.L. and Zhang X. Free vibration analysis of a three-dimensional soil-structure system *Earthquake Engineering and Structural Dynamics* Vol. 30, pp. 43-57, 2001.

[78] Wegner J.L., Yao M.M. and Zhang X. Dynamic wave-soil-structure interaction analysis in the time domain *Computer and Structures* Vol. 83, pp. 2206-2214, 2005.

[79] Wolf J.P. Soil-structure interaction with separation of base mat from soil (lifting-off) *Nuclear Engineering and Design* Vol. 38, No. 2, pp. 357-384, 1976.

[80] Wolf J.P. *Dynamic soil-structure-interaction* Englewood Cliffs, NJ: Prentice-Hall, 1985.

[81] Wolf J.P. *Soil structure interaction in the time domain* Prentice-Hall: Englewood Cliffs, NJ, 1988.

[82] Wolf J.P. Spring-dashpot-mass model for foundation vibrations *Earthquake Engineering and Structural Dynamics* Vol. 26, pp. 931-949, 1997.

[83] Wolf J.P. Response of unbounded soil in scaled boundary finite-element method *Earthquake Engineering and Structural Dynamics* Vol. 31, pp. 15-32, 2002.

[84] Wolf J.P. and Darbre G.R. Non-linear soil-structure interaction analysis based on the boundary-element method in time domain with application to embedded foundation *Earthquake Engineering and Structural Dynamics* Vol. 14, pp. 83-101, 1986.

[85] Wolf J.P. and Obernhuber P. Non-linear soil-structure-interaction analysis using dynamic stiffness or flexibility of soil in the time domain *Earthquake Engineering and Structural Dynamics* Vol. 13, pp. 195-212, 1985a.

[86] Wolf J.P. and Obernhuber P. Non-linear soil-structure-interaction analysis using Green's function of soil in the time domain *Earthquake Engineering and Structural Dynamics* Vol. 13, pp. 213-223, 1985b.

[87] Wolf J.P. and Skrikerud P.E. Seismic excitation with large overturning moments: tensile capacity, projecting base mat or lifting-off *Nuclear Engineering and Design* Vol. 50, pp. 305-321, 1978.

[88] Wolf J.P. and Song C. *Finite-element modelling of unbounded media* John Wiley & Sons Ltd 1996, West Sussex, England.

[89] Wu W.H., Wang J.F. and Lin C.C. Systematic assessment of irregular building-soil interaction using efficient modal analysis *Earthquake Engineering and Structural Dynamics* Vol. 30, pp. 573-594, 2001.

[90] Wegner J.L., Yao M.M., and Bhullar S.K. Dynamic wave soil structure interaction analysis of a two-way asymmetric building system DSSIA-3D *Journal of Engineering and Technology Research* Vol. 1 (2), pp. 026-038, May 2009.

[91] Zhang C., Chen X. and Wang G. A coupling model of FE-BE-IE-IBE for non-linear layered soil-structure interactions *Earthquake Engineering and Structural Dynamics* Vol. 28, pp. 421-441, 1999.

[92] Zhang X. and Liu Y. *Meshless method*. Tsinghua University Press & Springer, Beijing, 2004.

[93] Zhang X., Wegner J.L. and Haddow J.B. Unpublished SSWIA-3D manual, 1998.

[94] Zhang X., Wegner J.L. and Haddow J.B. Three dimensional soil-structure-wave interaction analysis in time domain *Earthquake Engineering and Structural Dynamics* Vol. 36, pp. 1501-1524, 1999.